Marine Geology 437 (2021) 106478

Contents lists available at ScienceDirect

Marine Geology

journal homepage: www.elsevier.com/locate/margo

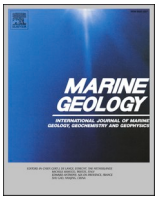

# Complex sedimentary processes in large coastal embayments and their potential for coastal morphological and paleo tropical cyclone studies: A case study from Choctawhatchee Bay Western Florida, U.S.A

P.N. Ranasinghe [a,b,*], J.P. Donnelly [b], R.L. Evans [b], J.R. Rodysill [c,b], N.U. Nanayakkara [a], P. J. van Hengstum [d,b], A.D. Hawkes [e,b], R.M. Sullivan [b,d], M.R. Toomey [c,b]

[a] Department of Oceanography and Marine Geology, Univerity of Ruhuna, Matara, Sri Lanka
[b] Geology and Geophysics, Woods Hole Oceanographic Institution, USA
[c] Florence Bascom, Geoscience Center, United States Geological Survey, Reston, VA, USA
[d] Department of Oceanography, Texas A&M University, Galveston, TX, USA
[e] Department of Earth and Ocean Sciences, University of North Carolina Wilmington, Wilmington, NC, USA

A B S T R A C T

Storminess and sea-level can both have a significant impact on landforms in cyclone-prone coastal regions, although much of our understanding comes from short-timescale modern observations. This study aims to understand the variability of sediment transport and deposition in the Choctawhatchee Bay/Santa Rosa Island in the northern Gulf of Mexico, establishing the dominant sediment transport processes and morphological response of the barrier system to long-term variations in storminess and rising sea-levels.

Here, we study the spatial and temporal changes in physicochemical properties of the sedimentary record of Choctawhatchee Bay to examine the character and fidelity of records of storm impacts spanning the Holocene. Proxies for marine and terrestrial conditions in the cores situated closer to the present barrier (proximal) show that sedimentation in coastal areas and marine influence of the bay during the last ~8000 yrs. were mainly determined by barrier response to the Holocene transgression and changes in storminess. In contrast, sedimentation close to the landward shore was governed by terrigenous input. The correlation of grain size and terrigenous proxies with regional hurricane records indicates that hinterland erosion by the rainfall during hurricane events is likely the dominant terrigenous sediment transport mechanism in areas close to the landward shore of the bay. These results suggest that sediment archives in large coastal deposition environments are equally suitable for sea level and cyclone modulated coastal morphological studies and paleo tropical cyclone studies, depending on the location, selected with an understanding of sedimentation processes in the vicinity.

## 1. Introduction

Tropical cyclones (TC) in the Indo-Pacific and hurricanes in the Atlantic pose a growing threat because of the increasing population and wealth in TC-prone areas (Pielke et al., 2008). Therefore, researchers are interested in determining the mechanisms governing TC frequency and intensity changes. Instrumental records span time intervals far too short to appropriately assess risk and understand the climatic forcing responsible for TC activity changes. In contrast, sediment archives preserved in various coastal depositional settings, such as coastal bays, lagoons, marshes, sinkholes, and blue holes on carbonate platforms, offer unique insights into the variability of storm activity over 1000's years. Knowledge of past storm patterns can help identify the forcing factors that control storminess, giving insights into potential future variability, which is a valuable asset for coastal management.

Site selection for paleo-TC studies is challenging because coastal systems are also undergoing complex changes in response to sea-level rise. Variations in storminess can also alter the sensitivity of a given site to storm impacts and influence the preservation potential of storm-induced deposits. For example, sediment supply and transport pathways may change, altering the character of storm-induced sediment transport and deposition (Sallenger Jr, 2000; Otvos, 2011). Storm surges are erosive events that can erode beach, dune, and barrier bars and back-barrier lowlands (Reimnitz and Maurer, 1979; Morton and Barras, 2011). During high-energy events, erosion can even remove portions of the sedimentary record (Morton, 2002; Eisemann et al., 2018). About 48 cm of sediment was eroded by hurricane Harvey which made landfall in 2017, in the San Jacinto Estuary (Du et al., 2019).

The well-developed Holocene sea-level and TC records of the northern Gulf of Mexico make Choctawhatchee Bay on the panhandle of

* Corresponding author at: Department of Oceanography and Marine Geology, Univerity of Ruhuna, Matara, Sri Lanka.
*E-mail address:* nalakaranasinghe@hotmail.com (P.N. Ranasinghe).

https://doi.org/10.1016/j.margeo.2021.106478
Received 28 January 2021; Received in revised form 3 April 2021; Accepted 6 April 2021
Available online 26 April 2021
0025-3227/© 2021 Elsevier B.V. All rights reserved.

Florida an ideal laboratory (Brandon et al., 2013; Lane et al., 2011; Rodysill et al., 2020 Milliken et al., 2008; Donnelly and Giosan, 2008to examine the effects of different coastal processes on the sediment record. Here, we studied the spatial and temporal changes in physicochemical properties of the sedimentary record of Choctawhatchee Bay (Fig. 1) to examine the character and fidelity of records of storm impacts spanning the Holocene.

### 1.1. Modern hydromorphology of choctawhatchee bay

Choctawhatchee Bay, FL is a drowned river valley system currently separated from the Gulf of Mexico by the Okaloosa peninsula and Santa Rosa Island (30.49°N, −86.58°W and 30.39°N, −86.10°W; Fig. 1). The bay opens to the Gulf of Mexico through "East Pass" (Destin Pass), which today is a nearly 500 m wide inlet at the east end of the Okaloosa barrier fronting the bay.

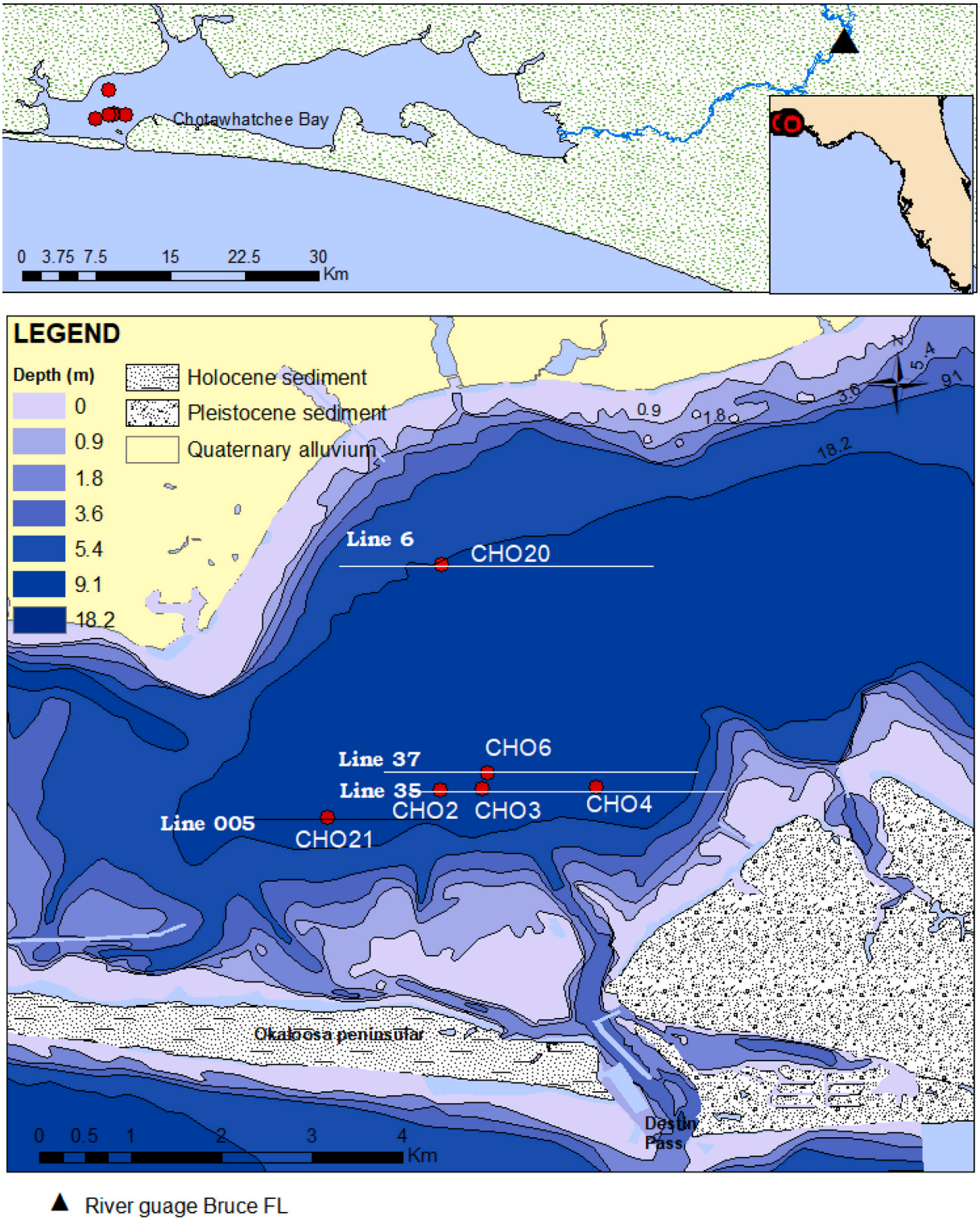


**Fig. 1.** Location of sampling sites in the Choctawhatchee Bay. Lines on the bottom image show shallow seismic (CHIRP) profiles . Geological formations are based on Otvos (1995) and the southeastern Geological society (2013).

According to data from Pensacola, FL, the area receives the highest rainfall during the summer (Jun-Sep) and winter (Jan-Mar) (NOAA). During most fall and winter, rainfall occurs in the region mainly associated with frontal systems from the northwestern United States. During most spring and summer, rainfall occurs mainly by convective processes and tropical storms (Baigorria et al., 2007). The Choctawhatchee River discharges into the bay about 37 km east of East Pass. Monthly discharge values at Bruce, FL (USGS 02366500) (Fig. 1) show that the Choctawhatchee River discharge is high during December – April, with the highest discharge in March. Annual discharge data for the period 1931–2017 show that annual discharge varied between 311 and 57 $m^3/s$. The tidal range within Choctawhatchee Bay is averaging 0.15 m (Ruth and Handley, 2006). Choctawhatchee Bay connects to Pensacola Bay by a narrow back-barrier channel formed behind Santa Rosa Island. According to Otvos (1985), over half of Santa Rosa Island is underlain by relict Pleistocene Gulfport formation made of barrier sand. Fort Walton Beach on the eastern portion of Santa Rosa Island is composed of Holocene sandy sediment. In contrast, the Okaloosa peninsula to the east of Destin Pass is largely the Pleistocene Gulfport formation.

### 1.2. Northern Gulf of Mexico sea-level history

While some investigators have argued for a complex Holocene sea-level history for the Gulf of Mexico, with a series of high and low stands (e.g., Tanner et al., 1992; Morton et al., 2000), dated sea-level indicators demonstrate that the region experienced a largely monotonic increase in sea level over the last 10,000 years (Milliken et al., 2008; Donnelly and Giosan, 2008) (Fig. 2). In general, the relative sea-level in the Gulf of Mexico increased about 20 m over the Holocene at a gradually decreasing rate. For example, the overall rate of rising over the last few millennia was only about 0.5 mm/year, compared to approximately 4 mm/year in the early Holocene (Milliken et al., 2008). According to the local tide gauge (Station 8,729,840, Pensacola, FL), the current sea-level rise rate over the last century is approximately 2.3 mm/year.

(https://tidesandcurrents.noaa.gov/sltrends/sltrends_station.shtml?id=8729840).

The barrier complexes of the Gulf of Mexico formed during the Holocene as post-glacial sea-level rise slowed down after around 5000 yrs. BP (e.g., Otvos Jr, 1970; Otvos, 1982; Otvos, 1985; Rodriguez et al., 2004; Rodriguez and Meyer, 2006; Törnqvist et al., 2004). Over the last 150 years, sea-level rise rates have increased dramatically in response to climate warming (e.g., Kemp et al., 2011), and sea-level rise is likely to accelerate as warming continues (Kopp et al., 2016). Moore et al. (2010) reveal that substrate composition, followed in rank order by substrate slope, sea-level rise rate, and sediment supply rate, are the most critical factors determining barrier island response to sea-level rise. Simple morphodynamic models suggest width and height drowning are the key modes of barrier failure in response to accelerated sea-level rise (Ashton and Lorenzo-Trueba, 2018). Because of the recent increase in the rate of sea-level rise, barriers may be more susceptible to breaching and overtopping during storm events today and into the future than they were 150 years ago. Studying sedimentological and geochemical changes in the proximal and distal sites to the barrier would reveal the barrier response to the sea level and its environmental impact on the bay, providing important clues about potential future changes in the system. Better constraints on the character of the evolution of back-barrier bay systems will provide important context for interpreting potential storm reconstructions from these environments.

### 1.3. Northern Gulf of Mexico tropical cyclone history

In the Gulf of Mexico, the most dominant types of severe storms are TCs. In contrast to the slowly decelerating rates of long-term sea-level rise, hurricane activity in the northeastern Gulf of Mexico appears to have changed significantly over the latter half of the Holocene (Fig. 2). Reconstructions of event beds likely related to hurricanes from coastal ponds and embayments in the northeastern Gulf of Mexico indicate significant centennial-scale variability within much of the last 4500 years, experiencing more frequent intense hurricane strikes than were suffered historically (Brandon et al., 2013; Lane et al., 2011; Rodysill et al., 2020; Fig. 2). In particular, the intervals between 4500 and 2300 years ago and 1500 and 700 years ago were much more active in terms of intense hurricane activity in the northeastern Gulf of Mexico than in the last 700 years (Lane et al., 2011; Brandon et al., 2013).

### 1.4. Choctawhatchee Bay tropical cyclone history

Over the last few decades, TC storm surges overwashed the western part of Santa Rosa Island and deposited sand sheets in Santa Rosa Sound. Several TCs significantly impacted the eastern Santa Rosa barrier island over the last few decades. Hurricane Dennis, which made landfall in 2005 as a Category-3 storm and created over 3 m surge at eastern Santa Rosa barrier; Hurricane Ivan, which made landfall in 2004 as a Category −3 hurricane and created 3–4 m storm surge; Hurricane Opal, which made landfall in 1995 as a Category −4 hurricane and created about 3 m

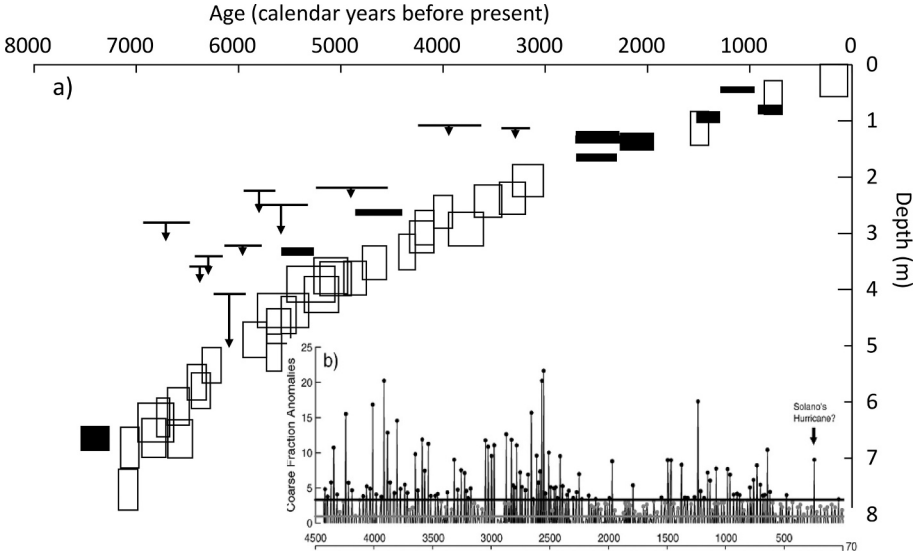


**Fig. 2.** Sea level and hurricane variability in in northwest Florida (Donnelly and Giosan, 2008), A: Sea-level data from the Mississippi delta (open boxes; from Törnqvist et al., 2006) and northwestern Florida (black boxes; Wright et al., 2005). Boxes represent age and vertical uncertainties. Bars with arrows are dated terrestrial samples from northwestern Florida, and length of the arrow represents vertical uncertainty. b). Coarse fraction anomaly plot of Mullet Pond Florida representing hurricane events (Lane et al., 2011).

surge (National Hurricane Center, 2012) are some of them. During Hurricane Ivan, extensive inundation and overwash occurred within 100 km from the storm center at landfall. Significant beach and dune erosion occurred as far as 300 km east of the storm center (Wang et al., 2006). The island morphology changed from a discontinuous foredune backed by hummocky back-barrier dunes and maritime forest (at the cuspate headlands) to washover terraces at the headlands and washover corridors between headlands (Houser, 2008).

Modern as well as Paleoclimate records for mid-late Holocene show tight coupling between the strength of El Ninò-Southern Oscillation (ENSO) and winter rainfall intensity (Donders et al., 2005; Cronin et al., 2002). Records show establishing modern ENSO frequency between 7000 and 5000 yrs. BP and increasing the ENSO intensification after 3500 yrs. BP (Donders et al., 2005). While the future of hurricane activity in the Gulf of Mexico is uncertain, basic theory (e.g. Emanuel, 1987), statistical relationships between large-scale climate parameters and TC activity(e.g., Mann et al., 2009), and downscaling global models (e.g., Emanuel, 2013; Knutson et al., 2007; Knutson et al., 2015) indicate that the intensity of TCs may increase as earth's climate continues to warm from increased concentrations of greenhouse gases in the atmosphere. Some studies have concluded that we already see an increase in the frequency of the most intense storms (Elsner et al., 2008; Kossin et al., 2013; Webster et al., 2005) and overall North Atlantic TC activity has increased over the last several decades. However, these conclusions have been challenged due to the brevity and inconsistency of the instrumental record (Landsea et al., 2006). Alternatively, Sobel et al. (2016) suggest that detectable TC activity trends will only emerge if greenhouse gas forcing continues to outpace anthropogenic aerosol-related cooling over the coming decades. Many modeling studies point toward increasing TC intensity over the coming century, but the significant regional variance is likely with some locations seeing an increase in the intensity of TCs and others seeing little change or even decrease inactivity. The modeling of Knutson et al. (2015) points toward more Category 4 and 5 TCs in the Gulf of Mexico by 2100 CE.

Detailed records of past hurricane activity are essential for understanding hurricane variability on multidecadal to centennial time scales. The main objective of this study is to understand the complex sedimentary processes in back-barrier depositional environments and fundamentally assess their potential for hurricane reconstructions using Choctawhatchee Bay, Florida, an ideal site to study such processes in a large hurricane-prone back-barrier bay.

## 2. Methods

### 2.1. Fieldwork

We mapped the subsurface strata in Choctawhatchee Bay with an Edgetech 512 (0.5–12 kHz) and 424 (4–24 kHz) Chirp shallow seismic systems from *RV Seminole* and *RV Arenaria*. Handheld GPS systems were used for navigation, and Kingdom Suite software was used to process and -visualize the Chirp data. An average seismic velocity of 1500 $ms^{-1}$ was used to convert the two-way travel time (TWT) to depth. The seismic and GPR surveys were used to scan the subsurface layers and identify undisturbed sediment sequence for coring (Figs. 1 and 3A).

Six coring locations (CHO2, CHO3, CHO4, CHO6, CHO20, and CHO21) were selected for analysis based on seismic mapping/imaging (Figures1 and 3A). Coring was carried out using a concrete vibrator vibracorer and hand-driven with rods (CHO2, CHO3, and CHO4) and a Rossfelder P-3 underwater electric vibracorer (CHO6, CHO20, and CHO21) to collect continuous sediment cores of 4–9 m in length. Cores were collected in water depths between 8 and 12 m. Sediment compaction and/or rodding was minimal, and core recovery was 89% - 99%. To ensure that we collected undisturbed sediment sequences near the surface. Hand-driven piston cores were collected with polycarbonate core tubes. Cores were sectioned in the field for transport, and they were split longitudinally in the lab for analysis and subsampling.

### 2.2. Laboratory analysis

All cores were stratigraphically logged, photographed, and radiographed (at 200 μm resolution) using ITRAX core scanner. The density contrast of sand and clay helps to identify the sand layers in radiographs. To understand the sea level influence and terrigenous input, chemical composition was determined at high resolution (1 mm) by scanning the cores with the X-ray Fluorescence Spectrophotometer (XRF detector) of the ITRAX core scanner having a Mo tube. Voltage was set for 30 kV, and 30 mA current was applied for 10 s exposure time. For this study, the four longest cores (CHO21, CHO3, CHO6, and CHO20) were selected for detailed analysis.

Visual and radiographs based core logging of the cores revealed that the sediment predominantly consists of siliciclastics. Loss on ignition (LOI) (Santisteban et al., 2004) analyses of selected test samples taken every 20 cm indicate organic content between 12 and 16% of the dry weight. Acid tests performed using 10% $HNO_3$ for samples taken at 20 cm intervals confirmed that sediment does not contain calcareous mud, and $CaCO_3$ was found only in the form of micro and macrofossils. Therefore, to characterize barrier overwash events and terrigenous erosional events, we measured the particle size of bulk sediments in cores at 1–2 cm resolution, using a Beckman Coulter LS13320 particle size analyzer. When selecting a sample for particle sizing, visible shells, organic fragments, particles >2 mm were manually removed.

Foraminiferal assemblage composition determined on the most landward core, CHO20, was used to understand the salinity changes associated with sea level and barrier changes. Approximately 1 $cm^3$ sample was taken at 20 cm intervals for analysis. Samples were washed through a 63 μm sieve and dried in an oven at 50 °C and again sieved through 125 μm and where the resultant larger fraction was used for analysis (>125 μm). Up to 200 foraminifera tests were picked (Patterson and Fishbein, 1989), identified, and counted for distributional analysis under a binocular microscope (4×). Online foraminifera identification guide (https://foraminifera.eu/) was used in the identification of species.

### 2.3. Statistical methods

A combined compositional data set was built using concentration data of nine elements (Cl, Fe, Ti, K, Ca, Se, Br, Sr, and Zr) for CHO 20, CHO21, and CHO6 sediment cores. Varimax Rotated Principal component analysis (PCA) was performed for the combined data set using the normalized concentrations of the above elements as variables to identify the key sources determining the chemical composition of the sediment. To examine whether distal and proximal sites can be separated based on chemical and grain size proxies, stepwise discriminant function analysis (DFA) was performed for the combined data set using the Mahalanobis distance classification method (Davis, 2002). The nine elements and grain size parameters d(10), d(50), and d(90) (The portion of particles with diameters smaller than d(10), d(50), and d(90 values were 10%, 50%, and 90% respectively) were treated as independent variables.

A set of statistical methods analyzed foraminiferal species distributions. R mode clustering was used to identify sub-assemblages or associations within the total living foraminiferal assemblage. Cluster Analysis was performed using Ward's method (Ward Jr, 1963) with combining minimum variance with a Euclidean distance based on the absolute abundance of the species. The results are displayed in a hierarchical dendrogram, indicating environmentally controlled associations (Osterman, 2003; Van Hengstum et al., 2008). PCA was used using foraminifera species as variables to verify the sub assemblages further. Varimax normalized rotation method was used and PCs with eigenvalues over one were extracted, and factor scores were used to explain the down-core variability of sub-assemblages,

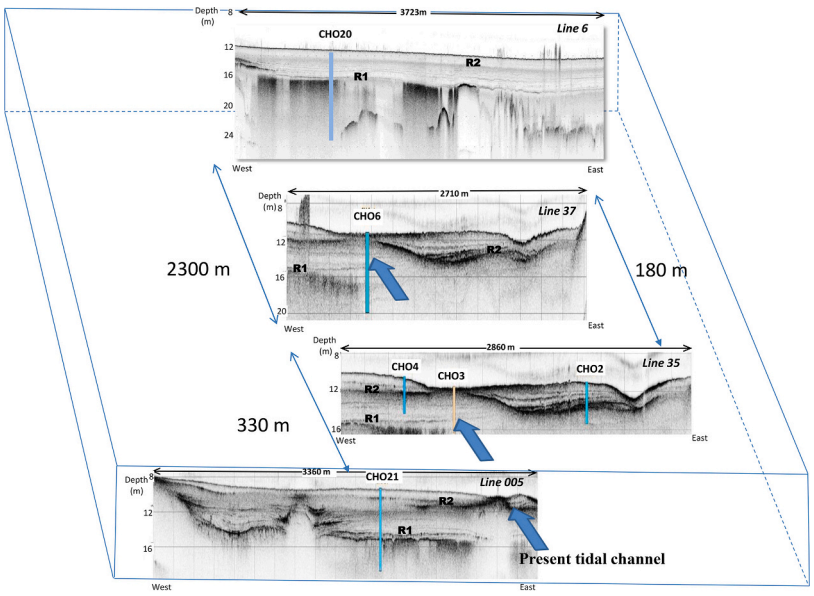


B

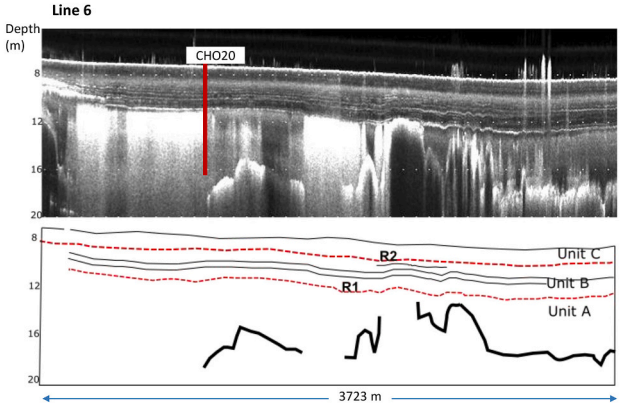


C

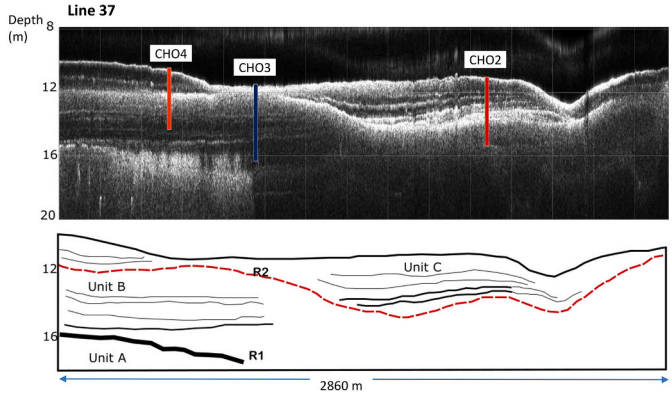


D

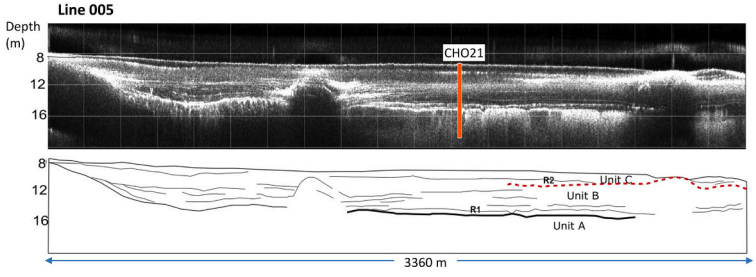


(caption on next page)

**Fig. 3.** A)- A 3-D view of the spatial locations of shallow seismic profiles across coring sites. Modern tidal channel path is marked by an arrow. B) Interpreted seismic profiles showing stratigraphic units A, B and C and reflectors. Lower boundary of Unit B and reflector showing basement reflector and erosional unconformity (dashed line) are marked as R1 and R2. Thickness of the interpreted lines represents the strength of the reflector.

### 2.4. Age determination

Mollusc shells (bivalve and gastropod) and wood fragments were extracted at various depths for radiocarbon dating. When available, we selected terrestrial plant fragments for dating. When no terrestrial material was available, we selected small mollusc shells (~1–5 mm), taking special care to avoid shells in sand layers to reduce the likelihood of dating reworked material. When present, we selected intact articulated shells to avoid transported material. In a few cases, we dated bulk organic samples if shells and terrestrial macrofossils were not present. The gas accepting ion source method (GAIS) is a rapid and low-cost radiocarbon dating method developed by the National Ocean Sciences Accelerator Mass Spectrometry (NOSAMS) facility of the Woods Hole Oceanographic Institution (Roberts et al., 2013). If 30 mg of carbonate sample was available, we used the GAIS method at NOSAMS for radiocarbon dating. Standard AMS techniques were used for age dating the other samples (Table 1). Since the $^{13}C$ value of an organic sample is indicative of whether it is derived from a marine or terrestrial environment, we used those values to select the radiocarbon calibration curve (Oehlert and Swart, 2014). Altogether, 51 samples were radiocarbon, dated from the six cores (Table 1).

Radiocarbon results of marine samples were calibrated for secular changes in atmospheric radiocarbon concentrations with the Marine 13 calibration curve (Reimer et al., 2013), using reservoir age of Map No

**Table 1**
Results of AMS and GAIS radiocarbon analysis. Calibrated ages and 2σ errors are given. Accession numbers begin with OS represent AMS dates while rest are GAIS. Numbers in italics were considered as outliers.

| Accession # | Core | Depth | Type | Age/yrs. BP | $\delta^{13}C$ | Cal age/yrs. BP | 2σ |
|---|---|---|---|---|---|---|---|
| 86,457 | CHO2 D2 2:5 86–87 cm | 186 | Mollusc | 3859 ± 126 | | 3823.5 | 342.5 |
| 86,458 | CHO2 D2 3:5 15–19 cm | 217 | Mollusc | 3582 ± 127 | | 3477.5 | 328.5 |
| 86,459 | CHO3 D2 5:5 1–4 cm | 451 | Mollusc | 4210 ± 125 | | 4286 | 359 |
| 86,460 | CHO3 D2 1:5 2–3 cm | 77 | Mollusc | 1333 ± 121 | | 888.5 | 245.5 |
| 86,461 | CHO3 D2 1:5 48–49 cm | 123 | Mollusc | 1066 ± 120 | | 655.5 | 212.5 |
| 86,462 | CHO3 D2 2:5 40–43 cm | 188 | Mollusc | 2753 ± 123 | | 2464 | 304 |
| 86,463 | CHO3 D2 3:5 50–51 cm | 300 | Mollusc | 3387 ± 128 | | 3216 | 327 |
| 86,464 | CHO3 D2 3:5 92.5–96.5 cm | 343 | Mollusc | 3519 ± 126 | | 3391.5 | 329.5 |
| 86,465 | CHO3 D2 4:5 51 cm | 400 | Mollusc | 3632 ± 125 | | 3541 | 320 |
| 86,466 | CHO3 D2 4:5 64–67 cm | 411 | Mollusc | 3696 ± 125 | | 3620.5 | 319.5 |
| *86,467* | *CHO3 D2 5:5 41.5–44 cm* | *492* | *Mollusc* | *3755 ± 126* | | *3692.5* | *326.5* |
| 86,468 | CHO3 D2 5:5 94.5 cm | 543 | Mollusc | 5618 ± 133 | | 5997.5 | 296.5 |
| 86,469 | CHO4 D2 1:3 65–69 cm | 151.5 | Mollusc | 791 ± 120 | | 706.5 | 75.5 |
| 104,590 | CHO21D1_3of4_87 cm | 642 | Mollusc | 4213 ± 100 | | 4278 | 293 |
| 104,591 | CHO21D1_4of4_II _47 cm | 794 | Mollusc | 5149 ± 102 | | 5496.5 | 227.5 |
| 104,592 | CHO21_D1_2of4_132 cm | 541 | Mollusc | 3531 ± 98 | | 3407 | 254 |
| *105,402* | *CHO20 D1 2:6 55 cm* | *180* | *Mollusc* | *7466 ± 23* | | *7914* | *79.5* |
| 105,403 | CHO20 D1 1:6 63 cm | 63 | Mollusc | 1121 ± 109 | | 700 | 192 |
| 105,404 | CHO20 D1 3:6 7 cm | 278 | Mollusc | 3583 ± 113 | | 3483 | 296 |
| 105,405 | CHO20 D1 4:6 60 cm | 475 | Mollusc | 4573 ± 115 | | 4765 | 545 |
| 105,406 | CHO20 D1 6:6 96 cm | 797 | Mollusc | 7653 ± 126 | | 8030 | 270 |
| 105,407 | CHO6 D2 1:5 84 cm | 84 | Mollusc | 891 ± 109 | | 478.5 | 186.5 |
| 105,408 | CHO6 D2 2:5 82 cm | 196 | Mollusc | 2904 ± 112 | | 2620.5 | 280.5 |
| 105,409 | CHO6 D2 3:5 48 cm | 302 | Mollusc | 3466 ± 113 | | 3316.5 | 296.5 |
| 105,410 | CHO6 D2 4:5125 cm | 523 | Mollusc | 4681 ± 115 | | 4930.5 | 328.5 |
| 105,411 | CHO6 D2 5:5 53 cm | 591 | Mollusc | 6248 ± 119 | | 6693 | 293 |
| 105,412 | CHO6 D3 5:6 21 cm | 636 | Mollusc | 6269 ± 120 | | 6718 | 299 |
| 105,413 | CHO6 D3 5:6133 cm | 748 | Mollusc | 6710 ± 122 | | 7196.5 | 261.5 |
| 105,418 | CHO2 D2 3:5 3 cm | 203 | Mollusc | 5491 ± 117 | | 5878 | 270 |
| 105,419 | CHO2 D2 3:5 74 cm | 274 | Mollusc | 3880 ± 113 | | 3848.5 | 312.5 |
| 105,420 | CHO2 D2 4:5 79 cm | 355 | Mollusc | 6568 ± 121 | | 7051.5 | 279.5 |
| 105,421 | CH02 D2 5:5 50 cm | 411 | Mollusc | 7330 ± 125 | | 7790.5 | 243.5 |
| 105,422 | CHO4 D2 3:3 55 cm | 385 | Mollusc | 3498 ± 113 | | 3364 | 297 |
| OS-90477 | CHO421–40 MICROC | 124 | Organic C | 1160 ± 25 | −19.5 | 1080.5 | 94.5 |
| OS-90622 | CHO421–40MACSH | 124 | Mollusc | 800 ± 25 | 0.2 | 413 | 84 |
| OS-90669 | CHO421–40MACOC | 124 | Plant/Wood | 285 ± 25 | −26.53 | 361.5 | 73.5 |
| OS-93962 | CHO21D21/3–105 cm | 105 | Mollusc | 820 ± 25 | 0.34 | 426 | 87 |
| OS-93963 | CHO21D22/3–61 cm | 177 | Mollusc | 1150 ± 25 | 1.37 | 700.5 | 65.5 |
| OS-94147 | CHO21D21/3–50 cm | 50 | Plant/Wood | 90 ± 30 | −26.53 | 143.5 | 121.5 |
| OS-94148 | CHO21D23/3–14 cm | 275 | Mollusc | 2810 ± 25 | −1.31 | 2550.5 | 139.5 |
| OS-94149 | CHO21D11/4–143 cm | 405 | Mollusc | 3360 ± 25 | −0.54 | 3215 | 116 |
| OS-94150 | CHO21D12/4–56 cm | 465 | Mollusc | 3450 ± 25 | 0.99 | 3311.5 | 102.5 |
| OS-94151 | CHO21D12/4–110 cm | 520 | Sediment Organic C | 4830 ± 30 | −25 | 5118 | 143 |
| OS-94174 | CHO21D13/4–43 cm | 618 | Plant/Wood | 28,100 ± 160 | −24.16 | 31,971 | 544 |
| OS-94175 | CHO21D14/4-I -38 cm | 733 | Mollusc | 5260 ± 30 | 1.24 | 5624.5 | 89.5 |
| OS-94176 | CHO21D14/4-II -94 cm | 841 | Mollusc | 6110 ± 40 | 0.02 | 6528.5 | 120.5 |
| OS-94314 | CHO21D13/4–128 cm | 683 | Mollusc | 5070 ± 35 | 0.87 | 5421 | 117 |
| OS-95165 | CHO3D21/5–49 cm | 124 | Mollusc | 1710 ± 30 | −1.48 | 1257 | 86 |
| OS-95258 | CHO20 D1 5:6–28 cm | 588 | Mollusc | 5910 ± 30 | 1.02 | 6322 | 87.5 |
| OS-95424 | CHO6D36/6–98 cm | 857 | Mollusc | 7400 ± 50 | 1.3 | 7847 | 123 |
| OS-96575 | CHO2_D2_2:5_96–97 cm | 196 | Mollusc | 3760 ± 30 | 0.5 | 3690 | 120 |

.

1782 (Hadden and Cherkinsky, 2015) (ΔR −3 and ΔR error 23), which was extracted from the Marine Reservoir ages database (Stuiver et al., 2020) for the Choctawhatchee Bay. Terrestrial samples were calibrated using the Intcal13 calibration curve (Reimer et al., 2013). Because sediment preserves signals of the bay-wide marine influence, we use Sr/Ti, a proxy for marine influence (Rasmussen et al., 2020), to correlate prominent features between sediment cores to generate a composite depth scale. The effect of syn and post-depositional processes, such as erosion, variable sedimentation rates, or sediment compaction during coring can be addressed using this technique. As a test of the correlation between the cores, $^{14}C$ dates can be transferred to the common depth scale (Darby et al., 2012 a). If the correlations are valid, then the CALIB calibrated $^{14}C$ data will plot along with a coherent, functional trend versus the composite depth scale. If the correlations are spurious, there will be no significant relationship between the composite depth scale and age (Darby et al., 2012). This age-depth relationship provides us with an objective means of determining which $^{14}C$ ages are valid and which are outliers.

Sr/Ti data from cores CHO3, CHO6, CHO21, and CHO20 were plotted as a function of depth, and the signals from each core were correlated by insertion of depth–depth tie points to core CHO 20 to develop the composite depth scale (Fig. 4). These cores have sandy silt to silt grain size variability, and the maximum compaction/rodding was 10%. Therefore, compaction/rodding was minimal and assumed to be uniform and progressive, as observed in homogenous sediment by Morton and White (1997). Since this correlation method addresses the effect of core compaction (Darby et al., 2012), no correction was made for compaction in constructing age models. When plotted, the $^{14}C$ dates on the composite depth scale yielded $r2 = 0.92$ for $n = 38$ valid AMS $^{14}C$ depth age pairs (Fig. 4) showing, a significant relationship between composite depths and ages. Therefore, a common age model for the western end of the bay was constructed using converted depths of the four cores CHO3, CHO6, CHO20, and CHO21 using R based WinBacon 2.2 software (Blaauw and Christen, 2013) (Fig. 4), which uses Monte Carlo techniques to reconstruct Bayesian accumulation histories. Results are represented as calibrated years before present (cal yrs. BP), of which 1950 CE is considered as the present by convention.

## 3. Results

### 3.1. Age model

The composite age model built using WinBacon software v. 2.2 (Blaauw and Christen, 2013) yielded bottom ages of ~7430 cal yrs. BP, 6770 cal yrs. BP, and 7430 cal yrs. BP, 6250 cal yrs. BP for CHO6, CHO21, CHO20, and CHO3 cores respectively (Fig. 4). Except for the slight decrease in sedimentation rate (~0.04 cm $yr^{-1}$) between ~1200–1900 cal yrs. BP and missing sediment above the R2 unconformity due to erosion (below describe under the results of the reflection seismic survey), sedimentation rates were almost constant (~0.1 cm $yr^{-1}$) during the last 8000 yrs. period. Calibrated radiocarbon ages are given in Table 1.

### 3.2. Reflection Seismic and grain size data

CHIRP shallow seismic profiles indicate the sub-bottom stratigraphy of Choctawhatchee Bay (Fig. 3). Seismic reflectors are formed due to the density contrast of layers at stratigraphic boundaries. Sand layers within silty sediment form strong acoustic reflectors, allowing us to identify barrier overwash derived sand layers through their reflectivity (Goff et al., 2005; Freeman and Roberts, 2013). Sand layers interpreted based on seismic profiles were verified using sediment cores. Three seismic stratigraphic units bounded by prominent reflectors were identified. Unit A, which has few individual reflectors visible, is found below the prominent reflector R1. Reflector R1 is found at around 6 m below the sediment surface at CHO21 and CHO4 core sites in seismic lines 35 and 5. Unit B, with a series of individual reflectors and having sandy sediment than unit A, is found between prominent reflectors R1 and R2. These individual reflectors may represent sand layers deposited by overwashing events. Reflector R2 exists about 1 m below the sediment surface at CHO3 in lines 35, cuts through the horizontal reflectors, and reached about 3 m depth at CHO2, providing evidence of an erosional unconformity. The same can be found in Line 37 as well. In Line 005, the R2 reflector is located about 3 m below the sediment surface. Based on CHIRP profiles, this unconformity is found in an area of about 2.4 $km^2$, and this erosional event scoured about 12 million cubic meters of sediment. Unit C also has a series of reflectors, including some prominent reflectors. In CHO4, Unit C is about 1.5 m thick.

When considering the stratigraphic relationship, grain size measurements in sediment cores CHO21, CHO4, CHO6, CHO3, and CHO2 confirm the presence of sandy layers at strong reflectors in seismic images (Fig. 5). Core CHO21, which is 561 cm in length, has silty sand between 200 and 290 cm (1200–2300 cal yrs. BP) and below 520 cm (3800 cal yrs. BP) (Fig. 5). Core CHO4 has a significant increase in sand content up to 135 cm (~360 cal yrs. BP) depth from the abrupt sand layer at 285 cm (Layer 3). Sand peaks (>40% sand) centered around 55 cm 165 cm, and 420 cm in the grain size plots are also evident in the grain size results of core CHO4 (Fig. 5).

CHO3, which was extracted from 400 m and 1100 m distances from CHO4 and CHO2 respectively, is 536 cm long, and 0–190 cm (top to-2500 cal yrs. BP), 360–430 cm (~3400–3600 cal yrs. BP), 480–536 cm (~3700–6000 cal yrs. BP) depth intervals have silty sand units (coarser-grained units) (Fig. 5). Other depth intervals composed of clayey silt units.

CHO6, which was extracted about 170 m north of CHO3, is 873 cm in length, has four stratigraphic intervals 0–200 cm (top to 2600 cal yrs. BP), 350–420 cm (~3600–4300 cal yrs. BP), 475–610 cm (~4800–6200 cal yrs. BP) and 685–775 cm (~6700–7400 cal yrs. BP)) of increased grain size (sandy silt units) (Fig. 5). The grain size pattern of the upper 550 cm of CHO6 is similar to that of CHO3. Radiographs well record distinct sand layers in sediment cores. Fig. 6 shows abrupt sand layers with sharp lower contacts between 122 and 252 cm section of the CHO6.

CHO2, extracted from the area where the erosional unconformity occurs about 2 m below the surface (Fig. 3), is 408 cm in length. Intervals 0–20 cm, 200–260 cm (~3500–3800 cal yrs. BP), and 410–470 cm (> ~ 7300) have coarser material (silty sand). Abrupt and broad grain size spikes centered around 60 cm and 330 cm depths are also evident in the grain size results of CHO2 (Fig. 5).

CHO20, which is the distal core, has coarse sand intervals at 119–148 cm (1100–1700 cal yrs. BP), 174–213 cm (2200–2600 cal yrs. BP), 582–598 cm (5600–5700 cal yrs. BP), 640–650 cm (6700–6800 cal yrs. BP), and 715–725 cm (7250–7350 cal yrs. BP) (Fig. 8).

Major event peaks (Layer 1–4) having significantly increased coarse fractions were identified after careful analysis of grain size distribution of individual layers.

### 3.3. Geochemistry

Principal component (PC) analysis identified 2 PCs explaining 76.8% of the total variability (Table 2a). XRF-PC1 has high correlations with Ca, Sr, and Zr, which are indicators for marine and beach sources (Carranza-Edwards et al., 2019; Goff et al., 2005) (Table 2b). XRF-PC2 has higher correlations with Fe, Se, Ti, and K, which are proxy elements of terrestrial sources (Gregory et al., 2015). XRF-PC1 scores are higher and XRF-PC2 lower in both CHO 6 and CHO21 sediment cores during the periods 3000–7000 cal yrs. BP and 300–1200 cal yrs. BP (Fig. 7), which likely indicates a higher degree of marine influence during these intervals (see discussion). Grain size follows XRF-PC1 in CHO6. In CHO20, XRF- PC1 has higher values during the periods 6000–7000, 3000–5400, and 100–1000 cal yrs. BP (Fig. 7). Unlike in CHO6, grain size follows XRF-PC2 in distal core CHO20.

Discriminant function analysis classifies distal sites with an accuracy

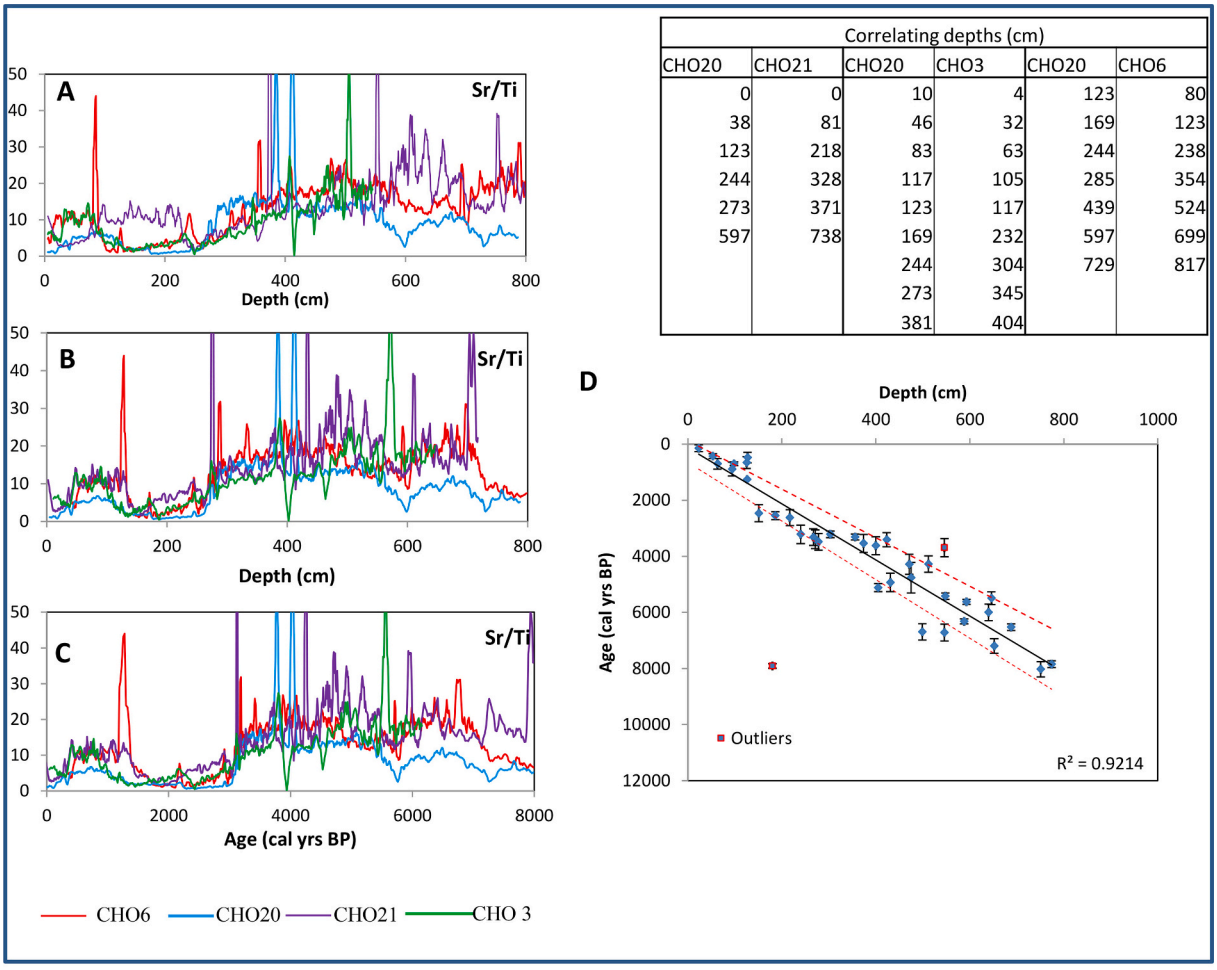


| Correlating depths (cm) | | | | | |
|---|---|---|---|---|---|
| CHO20 | CHO21 | CHO20 | CHO3 | CHO20 | CHO6 |
| 0 | 0 | 10 | 4 | 123 | 80 |
| 38 | 81 | 46 | 32 | 169 | 123 |
| 123 | 218 | 83 | 63 | 244 | 238 |
| 244 | 328 | 117 | 105 | 285 | 354 |
| 273 | 371 | 123 | 117 | 439 | 524 |
| 597 | 738 | 169 | 232 | 597 | 699 |
| | | 244 | 304 | 729 | 817 |
| | | 273 | 345 | | |
| | | 381 | 404 | | |

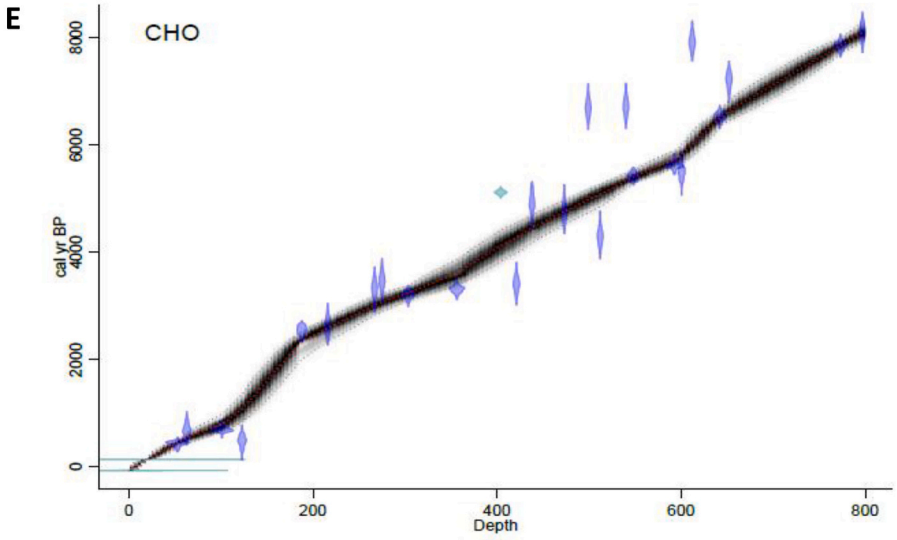


**Fig. 4.** Composite age model for Choctawhatchee Bay Fl. (A) Sr/Ti versus depth plots for CHO3, CHO6, CHO,21 and CHO20. Transfer functions were generated by correlating these Sr/Ti plots to interpolate them on to a common depth scale. (B) Sr/Ti versus interpolated depths of CHO3, CHO6 ad CHO21 . Depths were interpolated to CHO20 using the transfer functions(C). Correlation of Sr/Ti versus age plots of four cores obtained from both distal and proximal locations of the bay verify the accuracy of the regional age–depth model. (D). Correlation between interpolated depths vs ages . (E) of Age model constructed on CHO 20 depth scale using interpolated depths. Age model was constructed using Win Bacon 2.2 software Table shows the correlating depths of each core with CHO 20.

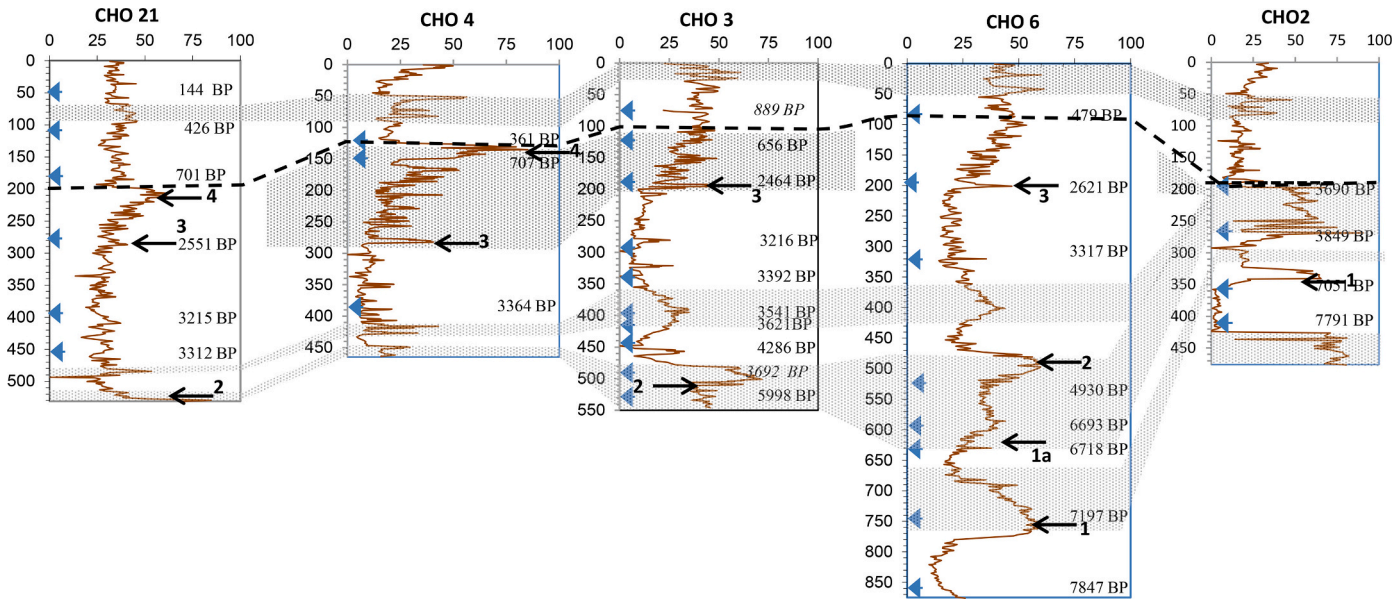


**Fig. 5.** Down-core (depth) variation of sand % (>63 υm) in sediment cores situated along proximal transects . CHO 4, CHO3, and CHO2 are situated along Seismic profile 2 (Fig. 3) and CHO 21 and CHO 6 are situated on seismic profiles 1 and 3. horizontally Calibrated ages are shown in BP and relevant depth is shown by an arrow. Shaded areas indicate periods of high energy conditions. Significant event beds are marked by hick arrows (Pls refer to text for the significance). Dash line shows the unconformity surface.

of 89.7% and proximal sites with an accuracy of 94.5% (Table 3). Structure matrix of DFA in which standardized beta coefficients are given for each variable in each discriminant (canonical) function, and the larger the standardized coefficient, the greater is the contribution of the respective variable to the discrimination between groups indicates that Fe, K, and D(90) have high coefficients for Function 1(Annex 1).

### 3.4. Foraminifera assemblages

A total of 32 species of foraminifera were identified in 43 sediment samples analyzed from CHO20. Twenty-four species with a relative abundance of >5% (>10 specimens per 200 individuals) in at least one sample were considered for statistical analysis. Taxa with unknown species were grouped into genera (*Elphidium spp, Ammonia spp, Bolivina spp, and Quinqueloculina spp*.), and less abundant species were grouped as minor spp. (Annex 2). A Factor analysis recognized three principal components (PC) having eigenvalues >1 (Table 4). These 03 factors explain 69.3% of the total variance. (Annex 3). The first component (PC1) explains 31.8% of the total variance, and *Nonionella atlantica*, *Quinqueloculina spp*, *Bolivina spp, and* minor *spp* show the highest correlation with PC 1. The second component (PC2) gain 21.4% of the total variance, and *Elphidium spp,* shows the highest positive correlation (0.562) while *Ammonia* spp. (−0.853) show the highest negative correlation. The third component (PC3) explains 16.1% with showing the highest positive correlation (0.895) with *Buliminella elegantissima* (Table 4). R mode cluster analysis recognized 3 clusters, and the dendrogram is shown in Annex 4. Combining the results of both cluster and PCA, 03 foraminiferal communities indicating three biofacies could be recognized (Table 5). Both cluster 1 and PC1 identify *Quinqueloculina*, *Bolivina*, *Nonionella atlantica* assemblage (*Quinq-Bolivn- Nonio),* which prefer higher salinities, between 25 and 40 PSU (Murray, 2006; Phleger, 1960; Poag, 2015). This assemblage was abundant between 3100 and 6500 cal yrs. BP (Fig. 9). Both Cluster 2 and PCA 2 identify *Elphidium* spp., which are abundant in brackish environments (Poag, 1981; Stewart et al., 1994; Debenay, 2000; Debenay and Guillou, 2002). PCA 2 scores were higher >7000 cal yrs. BP and started to decline after around 2000 cal yrs. BP. Organic-rich environments that preferred *Buliminella* spp. (Murray, 2006; Mamo et al., 2013; Abu-Zied et al., 2008; Buzas-Stephens et al., 2014) show the highest correlation with PCA 3 and forms Cluster 3. They were abundant before (~6000 cal yrs. BP) and after (3000 cal yrs. BP).

## 4. Discussion

The results of this study show how spatially varying coastal processes account for the variations in stratigraphy of the Choctawhatchee Bay (Fig. 10). Most stratigraphically continuous sand layers, present at the proximal locations to the barrier, are not found in the distal site situated toward the north of the bay. Instead, a separate sequence of sand layers can be found in the distal bay (Fig. 11). A prominent erosional unconformity, which is found at proximal sites, is represented only by a sand layer at the distal site. Grain size variability shows that sediment dynamics vary both spatial and temporarily. Nevertheless, as indicated by sediment chemistry and foraminifera assemblages, the temporal variability of marine influence is bay-wide.

### 4.1. Barrier dynamics and environmental changes in the proximal bay

Grain-size variability and chemical compositional changes in proximal sediment cores to the barrier provide clues as to how the barrier contributed to changing the bay's environment. CHO6 core has the longest record of grain size and chemical changes in the barrier's proximal environment.

#### 4.1.1. Flooding Choctwahtchee estuary during the Holocene transgression (8000–7000 cal yrs BP)

Increased terrigenous proxies and decreased marine chemical proxies in CHO6 indicate that the proximal environment of the present bay was a brackish coastal environment with more terrigenous input before 7500 cal yrs. BP. During the late Pleistocene, most modern rivers discharged down to the continental slope, and estuaries were situated on the current shelf (Tsandev et al., 2010; Törnqvist et al., 2006). Fluvial-deltaic deposition occurred on the modern shelf. When the sea-level started rising at the end of the last glaciation, these sediment depocenters migrated landward. Apalachicola estuary deltaic deposition occurred on the modern inner and mid-shelf between 10,000–7500 cal yrs. BP (Donoghue, 1993). Therefore, the terrigenous sediment-rich environment, reported in CHO6 before 8000 cal yrs. BP, likely

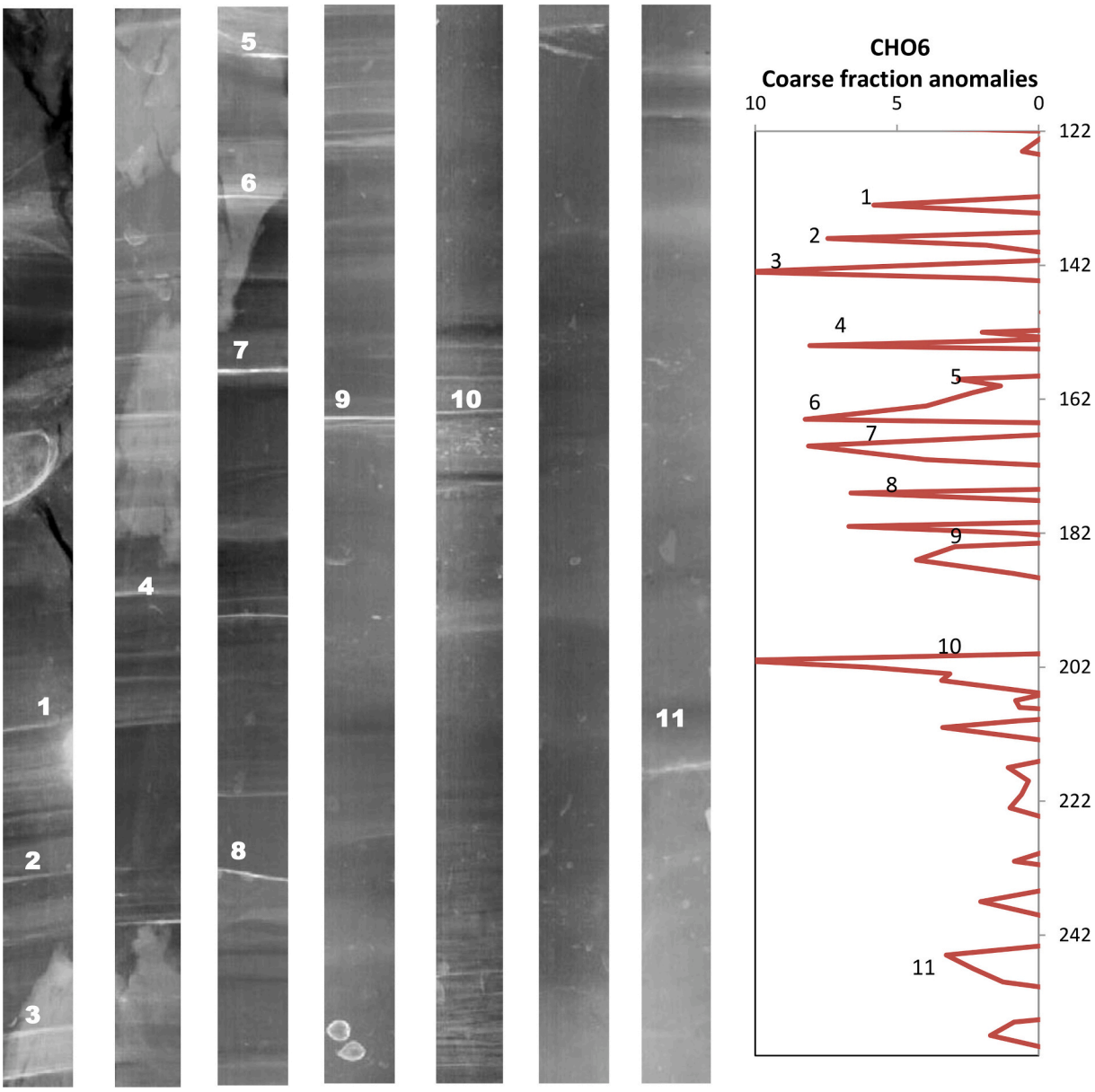


**Fig. 6.** X radiograph showing abrupt sand layers occur in between 122 and 252 cm depth interval in CHO6 sediment core. Corresponding sand layers are labeled in CHO6 coarse fraction anomaly plot.
No 10 layer shows the significant abrupt sand layer (Layer 3 in Fig. 5) occurred around 2600 cal yrs. BP.

represents the Choctawhatchee River estuary's gradual conversion during the Holocene transgression. Unit A, found below the strong reflector R1 in seismic profiles 1–4, has no distinct layering, but this coarse sandy sequence can likely be considered as the flooding surface (basement) of this paleo-estuary (Fig. 3). Deposition of sediment having geochemical, textural, and foraminiferal evidence for prevailed brackish conditions occurred in CHO6, CHO20, and CHO21 sites 8 m below the present bottom surface (−18 m present msl) before 7500 cal yrs. BP. When compared to the marine proxy values reported in recent sediment deposited at the present bay in CHO6, CHO2, and CHO20, it is clear that higher values which are found at the base of the cores indicate more brackish conditions prevailed before 7500 cal yrs. BP (Figs. 7 and 8). Sea-level rise in the Northern Gulf of Mexico area was relatively rapid between 8000 and 10,000 yrs. BP and reached −13-14 m present mean sea level at around 8000 yrs. BP (Milliken et al., 2008; Törnqvist et al., 2020). According to Otvos (2011) the Gulf level stood at -8 m before 7000 yrs. BP. Therefore, the chronology of this freshwater -brackish estuary stratigraphic sequence transition is compatible with the regional sea-level record.

About 1 m thick, shell-bearing, fining- upward sand layer (Layer 1) with sharp lower and upper contacts is found at 685–775 cm depth (~7000 cal yrs. BP) CHO6 core. A correlating >14 cm thick sand layer is found at 340 cm (326–340 cm) depth in CHO2 (Fig. 5). They might have been deposited by erosion and reorganization of a transgressive barrier by a possible storm event. A short period of decreased marine influence and lower sand content (Fig. 7) occurs above this sandy event bed (~6500 kyrs).

*4.1.2. Transition to a coastal plain estuary (between 7000 and 3500 cal yrs BP)*

This relatively low energy environment (i.e. less sand deposition) ended after another distinct sand layer occurred at 630 cm (Layer 1a) in CHO6 (Fig. 5). Breaching the transgressive barrier, likely by a storm event represented by layer 1a could have converted the partly closed

**Table 2**
Results of the PCA of XRF data

a. Total Variance Explained

| Component | Initial Eigenvalues | | | Extraction Sums of Squared Loadings | | | Rotation Sums of Squared Loadings | | |
|---|---|---|---|---|---|---|---|---|---|
| | Total | % of Variance | Cumulative % | Total | % of Variance | Cumulative % | Total | % of Variance | Cumulative % |
| 1 | 3.298 | 47.120 | 47.120 | 3.298 | 47.120 | 47.120 | 2.997 | 42.810 | 42.810 |
| 2 | 2.078 | 29.692 | 76.812 | 2.078 | 29.692 | 76.812 | 2.380 | 34.002 | 76.812 |
| 3 | 0.619 | 8.849 | 85.661 | | | | | | |
| 4 | 0.576 | 8.223 | 93.884 | | | | | | |
| 5 | 0.240 | 3.423 | 97.308 | | | | | | |
| 6 | 0.141 | 2.008 | 99.316 | | | | | | |
| 7 | 0.048 | 0.684 | 100.000 | | | | | | |

b. Rotated Component Matrix[a]

| Element | Component | |
|---|---|---|
| | 1 | 2 |
| K | 0.612 | **0.680** |
| Ca | **0.953** | −0.072 |
| Ti | 0.519 | **0.687** |
| Fe | −0.180 | **0.911** |
| Se | −0.044 | **0.762** |
| Sr | **0.951** | −0.090 |
| Zr | **0.712** | 0.147 |

Extraction Method: Principal Component Analysis. Rotation Method: Varimax with Kaiser Normalization.
a. Rotation converged in 3 iterations.

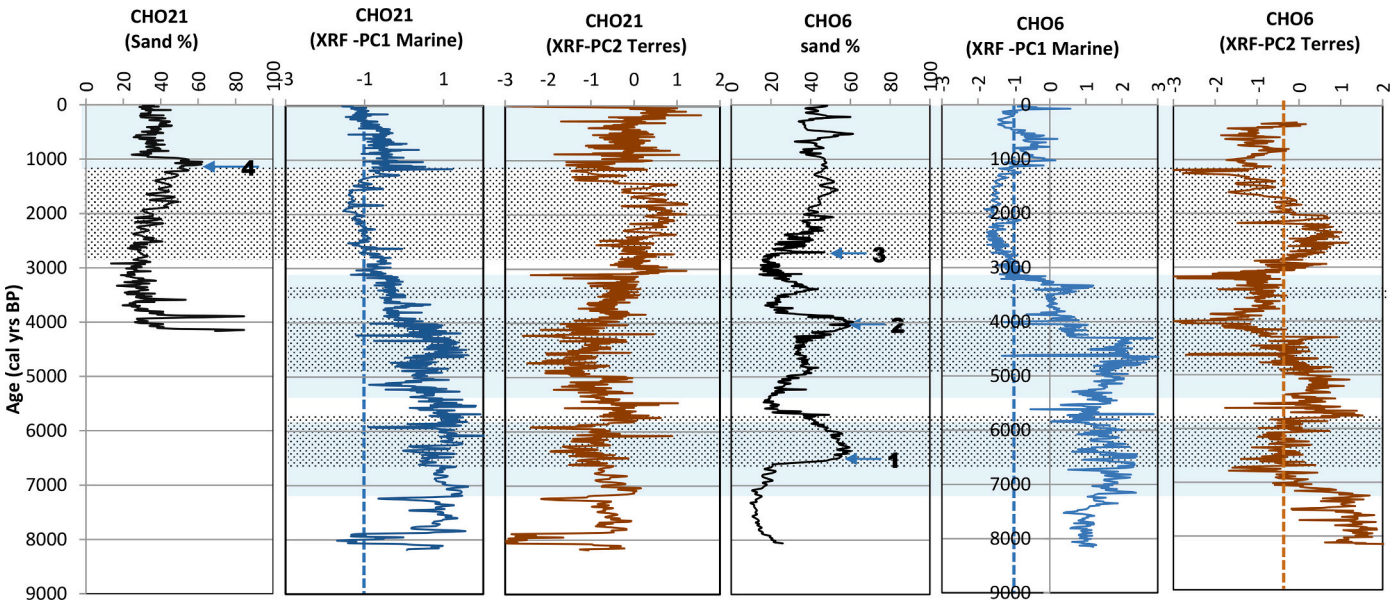


**Fig. 7.** Downcore variation of physiochemical properties in the two longest proximal cores (CHO21 and CHO6) . Intervals with higher marine proxies are shaded in plain blue while periods with increased sediment grain size are marked with a dotted shading. Dashed guide lines show proxy values of the modern barrier protected bay determined based on upper most values.

**Table 3**
Classification Results of Discriminant function analysis (DFA) performed to classify distal and proximal sites based on chemical and grain size of sediments.

| | | Group2 | Predicted Group Membership | | Total |
|---|---|---|---|---|---|
| | | | 1 | 2 | |
| Original | Count | Distal | 6905 | 795 | 7700 |
| | | Proximal | 716 | 12,366 | 13,082 |
| | | Ungrouped cases | 0 | 1298 | 1298 |
| | % | Distal | **89.7** | 10.3 | 100 |
| | | Proximal | 5.5 | **94.5** | 100 |
| | | Ungrouped cases | 0 | 100 | 100 |

a. 92.7% of original grouped cases correctly classified.

brackish estuary into an open coastal plain estuary, as evidenced by the subsequent more significant marine influence shown in Fig. 7. Another distinct 40 cm thick shell bearing sand layer (Layer 2) with sharp lower and upper contacts occurs in CHO21 (265–380 cm), CHO3 (478–510), and CHO6 (469–525 cm) (Fig. 5). Layer 2 occurs just after 4930 cal yrs. BP may represent an overwash event. This event is also followed by a short period of decreased sand accumulation. After this decrease in sand accumulation, sand content and marine indicators increase in CHO4, CHO3, and CHO6 cores between 4300 and 3400 cal yrs. BP(Figs. 5 and 7). Breaching the protective barrier could have resulted in this change at the proximal end of the bay. Unit B in seismic profiles (16–13 m) with clear intermittent reflectors may indicate this dynamic interval with sea-level rise, storm surges, and barrier migration occurred between ~7000–3400 cal yrs. BP (Fig. 3).

**Table 4**
– Rotated component matrix of the principal componenet analysis of formainifera species. Highligted species show the highest correlation with the relavent PC.

| Rotated Component Matrix[a] | | | |
|---|---|---|---|
| | Component | | |
| | 1 | 2 | 3 |
| *Buliminella elegantissma* | 0.104 | 0.092 | **0.895** |
| *Quinqueloculina spp* | **0.769** | 0.464 | −0.200 |
| *Elphidium spp* | 0.130 | **0.562** | 0.374 |
| *Ammonia spp* | −0.037 | −0.853 | −0.002 |
| *Bolivina spp.* | **0.766** | 0.047 | 0.257 |
| Minor spp. | **0.709** | −0.178 | 0.257 |
| *Nonionella atlantica* | **0.720** | 0.447 | −0.125 |

Extraction Method: Principal Component Analysis.
Rotation Method: Varimax with Kaiser Normalization.
a. Rotation converged in 10 iterations.

**Table 5**
Foraminiferal assemblages recognized by the PCA and cluster analysis and environments indicated by the recognized assemblages.

| Cluster Assemblage | Principal component | Clustered Species | Indication |
|---|---|---|---|
| Assemblage 1 (A1) | PCA 1 | *Nonionella atlantica* *Quinqueloculina spp.* *Bolivina spp* | ***Marine environments*** Gregory et al., 2015, Poag, 1981, Stewart et al., 1994, Debenay, 2000, Gischler et al., 2003, Hayward and Hollis, 1994, Hayward and Hollis, 1994, Murray, 2006 |
| Assemblage 2 (A2) | PCA 2 | *Elphidium spp.* | ***Brackish environment*** Poag, 1981, Debenay, 2000, Debenay and Guillou, 2002, Hayward and Hollis, 1994, Murray, 2006 |
| Assemblage 3 (A3) | PCA 3 | *Buliminella elegantissima* | ***Organic rich environments*** Gooday, 1993 |

#### 4.1.3. Transition to a bar-built estuary (3500 to 2500)

Grain size, chemical, and foraminiferal proxies indicate marine conditions significantly decreased during the period 2500–3000 cal yrs. BP, while clay and silty sediment, terrestrial input, and organic conditions increased (Figs. 7 and 9). Other than distinct episodic overwash sand layers, there was no significant sand supply into the bay during the interval 2500–3000 cal yrs. BP. Conversion of the transgressive barrier bar into a more stable barrier in response to the slowing down of sea-level rise around 4000–5000 cal yrs. BP (Milliken et al., 2008; Simms et al., 2007; Donoghue, 2011; Donnelly and Giosan, 2008) (Fig. 1) may have limited the connection between the Gulf and bay by 3000 cal yrs. BP (Fig. 10). Despite intermittent intense events, the storm frequency was generally lower in the Mullet Pond between 2800 and 3200 cal yrs. BP (Lane et al., 2011). This reduced storminess could have limited overwash and inlet formation converting the coastal plain estuary into a bar-built estuary. A new inlet might have formed to maintain the outflow of the Choctawhatchee River. However, geochemical and micropaleontological evidence shows reduced marine conditions during this period, suggesting any inlet was small and/or a significant distance from our area of study. Slowing sea-level rise and reduced storminess could have allowed forming a stable bay mouth barrier and reducing the marine influence to the bay by 3000 yrs. BP. Formation of the barrier island chain that forms the rim of the Apalachicola Bay, situated in northeastern Florida, and the building of deltas also started about 3000–4000 yrs. BP (Donoghue, 1993).

#### 4.1.4. Inlet formation and reestablishing the marine condition

Layer 3 is another distinct and continuous sand layer that occurs around 2500 cal yrs. BP in all proximal sediment cores (CHO21 at 280 cm, CHO4 at 280 cm, CHO3 at 200 cm and CHO6 at 200 cm) (Figs. 5 and 6). According to radiocarbon ages of CHO21, CHO3, and CHO6 cores, Layer 3 was deposited between ~2340–2900 cal yrs. BP, whereas Bayesian age models suggest an average age of 2326 ± 529 cal yrs. BP. Increased TC activity recorded during 2300–2800 cal yrs. BP in Mullet Pond (Lane et al., 2011) suggests that a surge from a strong TC could have deposited Layer 3 event bed. Sand supply in the proximal area of

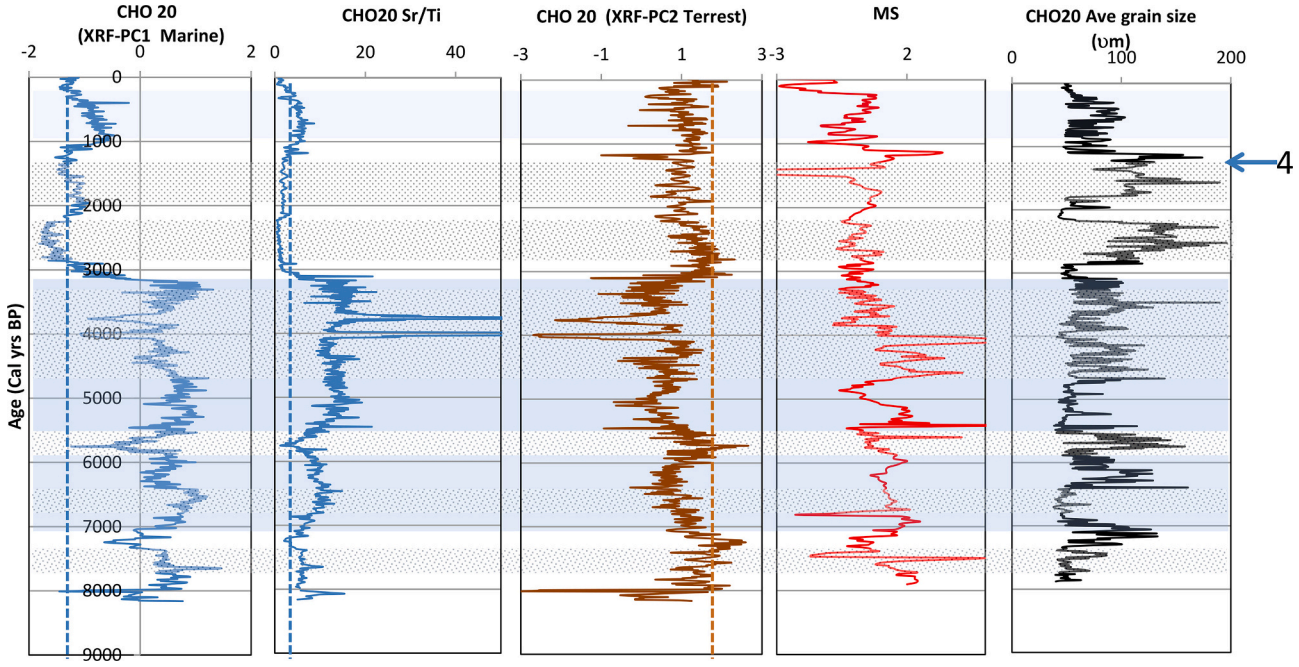


**Fig. 8.** Downcore variation of physiochemical properties in distal core CHO20. Intervals with higher marine proxies are shaded in plain blue while periods with increased sediment grain size are marked with a dotted shading. Event 4 which produced the R2 erosional event surface is marked by an arrow (4) on the grain size profile. Dashed guide lines show proxy values of the modern barrier protected bay determined based on upper most values. (For interpretation of the references to colour in this figure legend, the reader is referred to the web version of this article.)

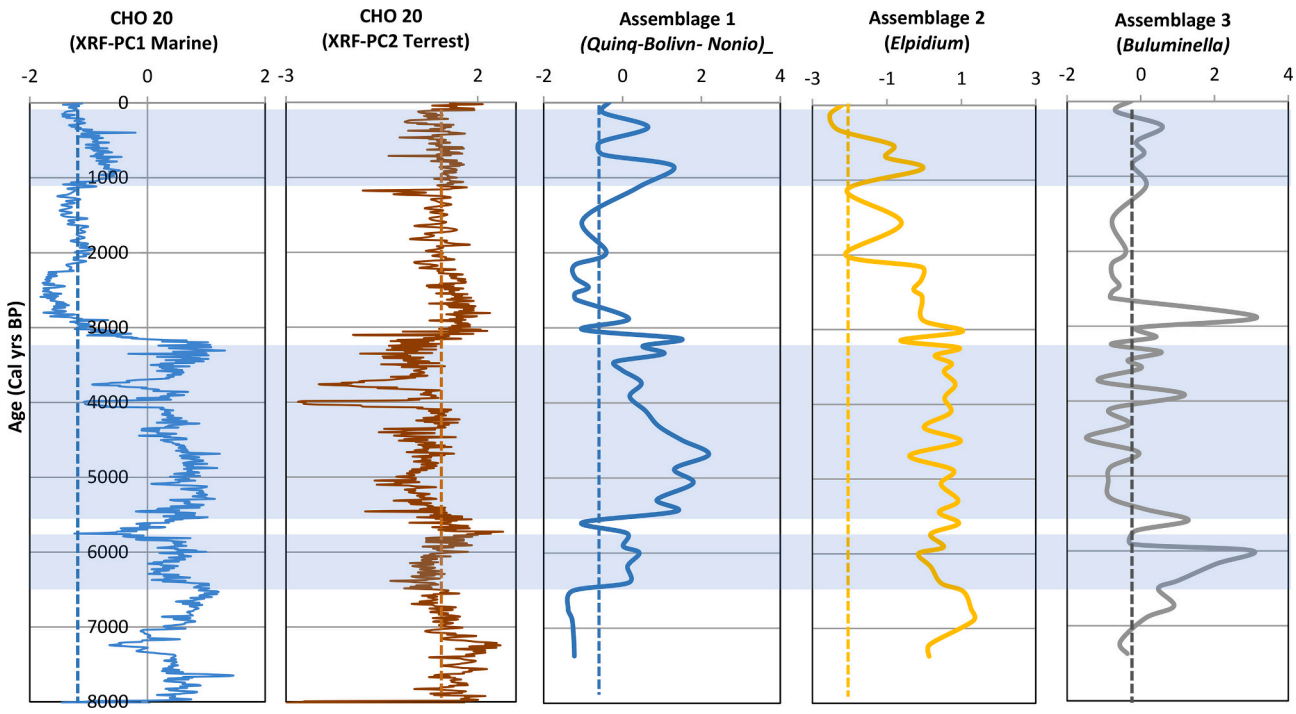


**Fig. 9.** Down core variability of relative abundance of foraminifera assemblages. in CHO20 Age axis is based on ages based on the Bacon age models. Shaded area shows the period of increased marine influence as shown by Assemblage 1 (Marine). Dashed guide lines show proxy values of the modern barrier protected bay determined based on upper most values.

the bay increased after this event, represented by Layer 3. Frequent sand layers between 1200 and 2600 cal yrs. BP(122–202 cm depth in CHO6) indicate that overwashing the weakened barrier or sediment transport through a new inlet formed by the Layer 3 event. However, the continuation of reduced marine conditions even after this event (Fig. 7) favours a weakened barrier rather than a new inlet formation.

A distinct sand layer (Layer 4) occurs between 1000 and 1500 cal ys BP in both proximal (CHO3 and CHO4) (Fig. 5) and distal cores (CHO20) (Fig. 8). Marine proxies show the establishment of present conditions between 1000 and 1500 cal yrs. BP (Fig. 7). Therefore Layer 4 may have been the result of an intense cyclone that breached the barrier, which might have become lower due to frequent overwash by surges during the 700–1500 cal yrs. BP stormy interval (Lane et al., 2011). Layer 4 chronologically correlates with a sand layer found above an erosional uniformity dated ~1050 cal yrs. BP at the Basin Bayou attached to the north side of the Choctawhatchee Bay at its east end (Rodysill et al., 2020). Therefore, this event must have propagated through the Choctawhatchee Bay, producing a strong storm surge.

#### 4.1.5. *The erosive unconformity*

R2 reflector, which occurs between 12 and 15 m depth from the water surface (2–3 m from sediment surface) in seismic profiles, truncates sediment in the vicinity of CHO2 (to 4000 yrs. BP level), providing evidence of an unconformity surface that likely resulted from a significant erosional event (Fig. 3). A thick sand layer, possibly a lag deposit, occurs at the unconformity in CHO21 and CHO4 (Fig. 5). The unconformity reaches close to the surface in CHO6 and CHO3. At these sites, the thickness of the sand layer is also thinner than in CHO21 and CHO4. Radiocarbon dates from CHO21 suggest that this scouring event occurred just before 700 ± 65 yrs. BP. In CHO4, a peak in the coarse fraction is found between 360 ± 73 and 710 ± 75 yrs. BP, while in CHO6 it lies just before 480 ± 187 cal yrs. BP. Therefore, we can assign 705 ± 99 yrs. BP for this event if we take the midpoint of the oldest upper date and the youngest lower date and propagate the uncertainty using a quadrature formula. Grain size plots of CHO21, CHO4, and CHO2 clearly show an abrupt change of grain size into clayey silt above the unconformity, indicating a depositional environment change to a low energy setting. Since tsunamis are unlikely in the region, this erosive event most probably resulted from a high magnitude storm surge produced by an intense TC. This surge could have easily encroached the coastal plain estuary through the inlet, scoured the bottom, and deposited the scoured material in the bay's distal areas. Funneling through the inlet and changing the flow characteristics to subcritical conditions, when surge overwash the barrier, can scour the bottom of the bay. The depression formed by the erosional event was subsequently filled with sediment, brought by sediment transport processes such as currents and storm surges. No erosional uniformity is found at the CHO20 site, and this event is represented by a 4 cm sand layer that occurred at 60–63 cm depth (Fig. 8).

#### 4.1.6. *Establishing present condition- back to a bar-built estuary*

As discussed above, a significant decrease in sedimentation is observed after R2 at CHO6 and CHO3, while other proximal sites record a significant decrease in sand content. This fine-grained sediment deposition continues till the present, indicating that the present-day barrier configuration was established after this erosive event at 700 yrs. BP. The movement of the tidal inlet across CHO3 and CHO6 (Fig. 3A) could have reduced sedimentation in the area. Unit A in seismic stratigraphy profiles, which is thinner and consists of coarser sediment on this unconformity surface in CHO3 and CHO6 region, also indicates reduced sediment deposition and higher energy conditions (Fig. 3). Therefore, we can identify this region as the modern tidal inlet of the bay. An increase in grain size is observed during the last 300 yrs.

### 4.2. *Environmental changes in landward reaches of the bay and tropical cyclone variability*

Geochemical proxy data for marine conditions (XRF PC1 and Sr/Ti) and foraminifera relative abundance data show that the distal site (CHO20) also responded to the environmental changes in the bay due to barrier dynamics resulted from sea-level rise and TC activity. In contrast, proxies for terrigenous input and particle size in the CHO20 show that

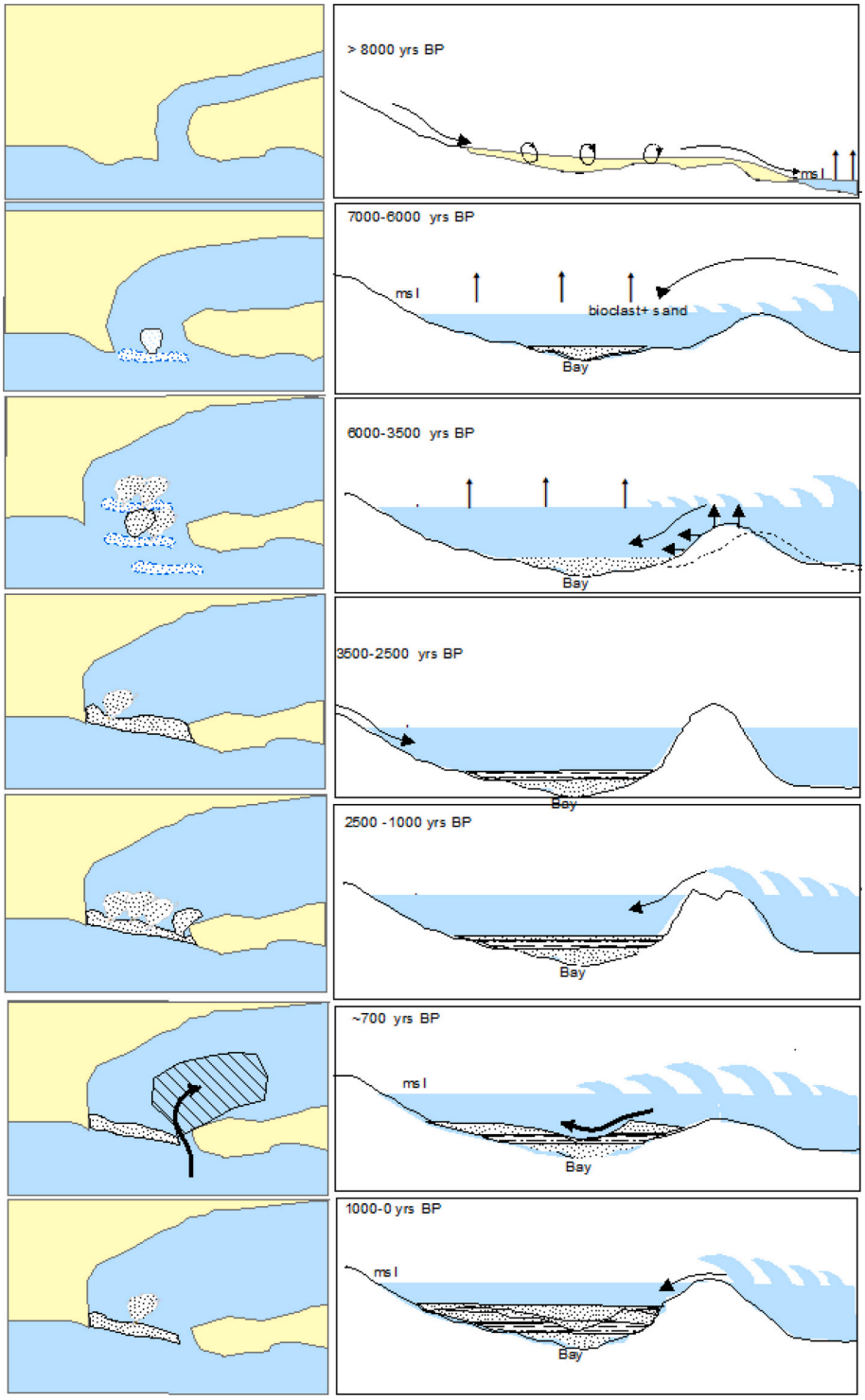


**Fig. 10.** A cartoon showing the morphological changes in the Choctawhatchee Bay through the last 8000 yrs. Figs. 1a-7a show the changes in the plan view. Figs. 1b-7b show the cross sectional view of changes in barrier related sedimentation. 1a-1b – Former Choctawhatchee river estuary 2a-2b- Gradual marine flooding due to sea level transgression. Over-washing of the transgressive barrier forms over-wash fan deposits. 3a-3b –Conversion to a coastal plain estuary. Formation of over-wash fans by hurricane events and migration of the transgressive barrier control the sedimentation. 4a-4b. – Conversion to a bar-built estuary after sea level stabilization. Closure of the western inlet restricted marine influence. 5a-5b –Frequent over-wash events during the intense hurricane active interval make the barrier weaker, leading to form a new inlet. 6a-6b – Intense hurricane event scoured the bottom of the bay. 7a-7b- Establishing the present conditions through the new inlet formation.

sedimentary processes in the distal bay are not sensitive to the barrier changes. The structure matrix of Discriminant Analysis also shows that terrigenous input and silt/clay have the highest correlation to Discriminant Function1 (DFA 1), identifying them as the most useful components in distinguishing distal and proximal sites.

#### 4.2.1. *Changes in the estuary environment*

In CHO20, brackish environments preferred *Elphidium* foraminifera assemblage (PC2) (Debenay, 2000; Debenay and Guillou, 2002; Hayward and Hollis, 1994) became abundant around 7000 cal yrs. BP. Geochemical proxies of CHO20 were reached higher than the modern values before 8000 cal yrs. BP (Fig. 8). This evidence indicates that marine flooding of the freshwater dominant landward reaches of the former Choctawhatchee estuary during the Holocene transgression (Figs. 7–9). The abundance of the saline water (25–40‰) preferred *Nonionella-Quinqueloculina-Bolivina* assemblage (Debenay, 2000; Debenay and Guillou, 2002; Gischler, 2003; Hayward and Hollis, 1994; Murray, 2006) began to increase around 6500 cal yrs. BP (Figs. 8-9) providing evidence for the onset of the gradual transformation of the brackish estuary into a more saline estuary.

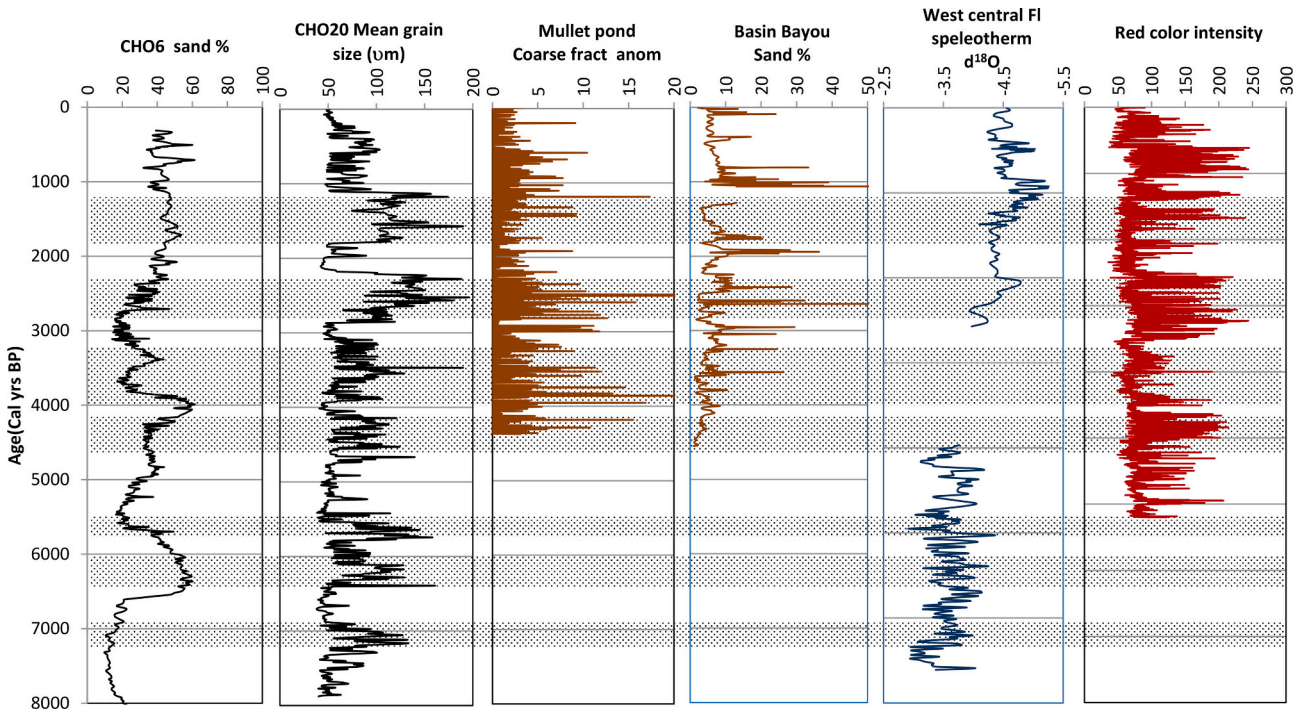


**Fig. 11.** Correlation of grain size variability in distal core with the regional cyclone record by Lane et al., 2011 Rodysill (in prep). The CHO 20 record does not correlate with the red colour intensity (ENSO) record (Moy et al. 2002) or west central Florida record (Soto 2005, Pollock et al. 2016)) but correlate with regional cyclone records. The Proximal record (CHO6) does not correlate with any other records. (For interpretation of the references to colour in this figure legend, the reader is referred to the web version of this article.)

Marine chemical proxy records show higher variability at the distal site than the proximal sites showing higher sensitivity to changes in salinity conditions. A significant decrease in marine conditions is recorded around 5600 and 1000–3000 cal yrs. BP (Fig. 7–9). A decrease in *Nonionella-Quinqueloculina-Bolivina* assemblage and a significant decrease in geochemical proxies, and the increase in terrestrial proxies clearly show that salinity decreased and accumulation of terrestrial matter increased during the above intervals. Geochemical and foraminifera proxies show that the salinity increased and present conditions gradually established after around 1000 cal yrs. BP. Figs. 7–9).

Grain-size variability in the distal core CHO20, which has a different pattern than the core locations closer to the barrier, shows increased grain size centered around 7300, 6500, 5500, 3700, 2500, and 1000 cal yrs. BP (Fig. 8). Some of these intervals with larger grain size positively correlate ($r > 1$) well with terrestrial proxies (XRF PC2), suggesting that these intervals have a terrestrial origin in contrast to the barrier origin of the sand layers in the proximal sites (Fig. 8). Grain size and terrestrial proxies (XRF-PC2) of CHO20, as well as Mullet Pond coarse fraction anomalies positively correlate with west-central Florida precipitation record dominated by TC, convection and frontal rainfall (Baigorria et al., 2007), providing evidence for increased supply of sand by enhanced precipitation during TC cyclone active intervals.

#### 4.2.2. *Cyclone history in preserved landward sediment deposits*

Increased TC active periods recorded in Mullet Pond between 2300 and 2800 cal yrs. BP and 600–1500 cal yrs. BP in Basin Bayou and Shotgun Pond FL (centered at 1000 cal yrs. BP) (Rodysill et al., 2020) and Spring Creek, FL (centered around 1000 cal yrs. BP) (Brandon et al., 2013) correlate with increased grain size periods centered around 1000 and 2500 cal yrs. BP in CHO20 (Fig. 10), implying that coarse terrigenous input is related to extreme precipitation driven by TCs. Therefore, grain size peaks at this distal site cannot be from overwash fans of storm surges. They are more likely deposited from hinterland erosion during heavy TC driven precipitation or landward shore erosion by large waves generated by TC due to east-west fetch of the bay.

## 5. Potential for paleo-hurricane studies in large coastal depositional environments

Although paleo-hurricane studies are conducted in TC belts, using sedimentary archives in various coastal and marine depositional environments, the suitability of these environments to isolate signatures of TCs has to be identified with utmost care. Sedimentary archives only preserve evidence of events that exceed the local intensity threshold necessary to transport and deposit coarse-grained material to the particular back-barrier environment. For example, Salt Pond, a coastal pond in Falmouth MA, USA, records only severe TCs (Donnelly et al., 2015). Donnelly and Woodruff (2007) show that sites closer to barriers in Laguna Playa Grande (LPG), Vieques, Puerto Rico are also not suitable to construct hurricane records because proximal sites to the barrier can receive sediment from localized breaching by less intense events. Such sites are also susceptible to erosion and truncation of the sediment record by over-washing and inlet processes. Liu and Fearn (2000) argued that both very close to the shore and very far from the shore locations in coastal lakes are not favorable to isolate storm surge events.

Choctawhatchee Bay is a suitable environment to assess the spatial potential of a large, bar built estuary to construct long TC records. Grain size variability since the mid-Holocene, in the proximal areas of the barrier bar, indicates that energy changes in the environment are driven by the barrier dynamics, which is controlled by both TC and sea level rise, making it difficult to isolate the TC signal. Changes in sand deposition due to the presence or absence of a barrier, sea-level related barrier movement, hiatuses in the record due to erosion by extreme events are some of the processes making the construction of a TC record difficult. However, as discussed above, distal sites within the bay, away from other sediment transport processes such as barrier migration and river discharge to the bay, are more suitable to construct TC records. However, locations very close to the landward shore may also not be suitable because there is a high possibility for sand deposition from bank erosion, even during moderate local wave/rain events.

Similarly, locations proximal to streams or rivers may not be

conducive due to sand supply during and after rainfall events. Therefore, mid-bay locations, away from the barrier and river input but close enough to deposit sand by TC related extreme precipitation events, can help reconstruct long TC records of the Gulf of Mexico. However, basin size, river input, and topography have to be considered when selecting the sampling sites.

## 6. Conclusions

Grain size, physicochemical, and micropaleontological proxies provide insight into the evolution of Choctawhatchee Bay during the Holocene. Frequent overwashing of the transgressive barrier was the main sediment transport mechanism into the bay during this Holocene transgression. After the Holocene sea-level transgression gradually submerged the former estuary of the Choctawhatchee River, it was transformed into an open coastal plain estuary between 6000 and 7000 cal yrs. BP. Its saline conditions prevailed until a stable barrier bar was established between 3500 and 4000 cal yrs. BP due to slowing down post-deglacial relative sea-level rise and decreasing storminess. The stable mouth bar (barrier) potentially converted the Choctawhatchee bay into a bar-built estuary and isolated from the Gulf of Mexico by around 3000 cal yrs. BP. Possible inlet formation by a storm surge of an intense hurricane made landfall around 2500 cal yrs. BP, reconnected the bay to the Gulf. More frequent overwash of the barrier by TCs during the stormy period between 700 and 1500 cal yrs. BP may have further weakened the barrier. The present condition was established in the bay when a significant barrier erosion event occurred between 1000 and 1300 cal yrs. BP, which correlates with an erosive event recorded at Basin Bayou at the northern end of the bay. A similar erosive event, which is most probably a high magnitude storm surge of an intense hurricane, has scoured about 2 m sediment in about 2.4 $km^2$ area at around 705 ± 99 yrs. BP. Such strong erosive surges by TCs, irrespective of the distance from the beach, is a vital process that needs to be studied in detail. Even though barrier dynamics controlled marine influence throughout the bay, sediment processes were area-specific and controlled by single or multiple processes such as barrier dynamics, shore and hinterland erosion, and streams discharge. The proximal areas of such large bar built estuaries in hurricane-prone areas are not suitable for constructing paleo tropical cyclone records due to sediment transport related to sea-level related barrier dynamics. However, distal areas in such coastal systems, away from stream inlets, may provide suitable sediment archives preserving event signals produced by hinterland erosion from hurricane rainfall.

## Declaration of Competing Interest

None

## Acknowledgements

This study was financially supported by SERDP RC-1702 research grant. Authors especially thank Stephanie Madison for coordinating field and laboratory work. We thank Dr. Andrew Ashton for helping in the field. Any use of trade, firm, or product names is for descriptive purposes only and does not imply endorsement by the U.S. Government.

## Appendix A. Supplementary data

Supplementary data to this article can be found online at https://doi.org/10.1016/j.margeo.2021.106478.

## References

Abu-Zied, R.H., Rohling, E.J., Jorissen, F.J., Fontanier, C., Casford, J.S., Cooke, S., 2008. Benthic foraminiferal response to changes in bottom-water oxygenation and organic carbon flux in the eastern Mediterranean during LGM to recent times. Mar. Micropaleontol. 67 (1–2), 46–68.

Ashton, A.D., Lorenzo-Trueba, J., 2018. Morphodynamics of barrier response to sea-level rise. In: Barrier Dynamics and Response to changing climate. Springer, Cham, pp. 277–304.

Baigorria, G.A., Jones, J.W., O'Brien, J.J., 2007. Understanding rainfall spatial variability in Southeast USA at different timescales. Int. J. Climatol. 27 (6), 749–760.

Blaauw, M., Christen, J.A., 2013. In: Bacon Manual e v2. 2, Blaauw, M., Wohlfarth, B., Christen, J.A., Ampel, L., Veres, D., Hughen, K.A., Preusser, F., et al. (Eds.), (2010),—Were last glacial climate events simultaneous between Greenland and France, pp. 387–394.

Brandon, C., Woodruff, J.D., Lane, P., Donnelly, J.P., 2013. Constraining flooding conditions for prehistoric hurricanes from resultant deposits preserved in Florida sinkholes. Geochem. Geophys. Geosyst. 14, 2993–3008.

Buzas-Stephens, P., Livsey, D.N., Simms, A.R., Buzas, M.A., 2014. Estuarine foraminifera record Holocene stratigraphic changes and Holocene climate changes in ENSO and the north American monsoon: Baffin Bay, Texas. Palaeogeogr. Palaeoclimatol. Palaeoecol. 404, 44–56.

Carranza-Edwards, A., Kasper-Zubillaga, J.J., Martínez-Serrano, R.G., Cabrera-Ramírez, M., Rosales Hoz, L., Alatorre Mendieta, M.A., Márquez-García, A.Z., Lozano-Santa Cruz, R., 2019. Provenance inferred through modern beach sands from the Gulf of Tehuantepec, Mexico. Geol. J. 54 (1), 552–563.

Cronin, T.M., Dwyer, G.S., Schwede, S.B., Vann, C.D., Dowsett, H., 2002. Climate variability from the Florida Bay sedimentary record: possible teleconnections to ENSO, PNA and CNP. Clim. Res. 19 (3), 233–245.

Darby, D.A., Ortiz, J.D., Grosch, C.E., Lund, S.P., 2012. 1,500-year cycle in the Arctic Oscillation identified in Holocene Arctic Sea-ice drift. Nat. Geosci. 5 (12), 897–900.

Davis, C.J., 2002. Statistics and Data Analysis in Geology, 3rd edition. John Wiley and Sons, New York.

Debenay, J.P., 2000. Foraminifers of paralic tropical environments. Micropaleontology 46, 153–160.

Debenay, J.P., Guillou, J.J., 2002. Ecological transitions indicated by foraminiferal assemblages in paralic environments. Estuaries 25 (6), 1107–1120.

Donders, T.H., Wagner, F., Dilcher, D.L., Visscher, H., 2005. Mid-to late-Holocene El Nino-Southern Oscillation dynamics reflected in the subtropical terrestrial realm. Proc. Natl. Acad. Sci. 102 (31), 10904–10908.

Donnelly, J.P., Giosan, L., 2008. Tempestuous highs and lows in the Gulf of Mexico. Geology 36 (9), 751–752.

Donnelly, J.P., Woodruff, J.D., 2007. Intense hurricane activity over the past 5,000 years controlled by El Niño and the West African monsoon. Nature 447 (7143), 465–468.

Donnelly, J.P., Hawkes, A.D., Lane, P., MacDonald, D., Shuman, B.N., Toomey, M.R., van Hengstum, P.J., Woodruff, J.D., 2015. Climate forcing of unprecedented intense-hurricane activity in the last 2000 years. Earth's Future 3 (2), 49–65.

Donoghue, J.F., 1993. Late Wisconsinan and Holocene depositional history, northeastern Gulf of Mexico. Mar. Geol. 112 (1–4), 185–205.

Donoghue, J.F., 2011. Sea level history of the northern Gulf of Mexico coast and sea level rise scenarios for the near future. Clim. Chang. 107 (1-2), 17.

Du, J., Park, K., Dellapenna, T.M., Clay, J.M., 2019. Dramatic hydrodynamic and sedimentary responses in Galveston Bay and adjacent inner shelf to Hurricane Harvey. Sci. Total Environ. 653, 554–564.

Eisemann, E.R., Wallace, D.J., Buijsman, M.C., Pierce, T., 2018. Response of a vulnerable barrier island to multi-year storm impacts: LiDAR-data-inferred morphodynamic changes on Ship Island, Mississippi, USA. Geomorphology 313, 58–71.

Elsner, J.B., Kossin, J.P., Jagger, T.H., 2008. The increasing intensity of the strongest tropical cyclones. Nature 455 (7209), 92–95.

Emanuel, K.A., 1987. The dependence of hurricane intensity on climate. Nature 326 (6112), 483–485.

Emanuel, K.A., 2013. Downscaling CMIP5 climate models shows increased tropical cyclone activity over the 21st century. Proc. Natl. Acad. Sci. 110 (30), 12219–12224.

Freeman, A.M., Roberts, H.H., 2013. Storm layer deposition on a coastal Louisiana lake bed. J. Coast. Res. 29 (1), 31–42.

Gischler, E., 2003. Holocene lagoonal development in the isolated carbonate platforms off Belize. Sediment. Geol. 159 (1–2), 113–132.

Gischler, E., Hauser, I., Heinrich, K., Scheitel, U., 2003. Characterization of depositional environments in isolated carbonate platforms based on benthic foraminifera, Belize, Central America. Palaios 18 (3), 236–255.

Goff, J.A., Mayer, L.A., Traykovski, P., Buynevich, I., Wilkens, R., Raymond, R., Glang, G., Evans, R.L., Olson, H., Jenkins, C., 2005. Detailed investigation of sorted bedforms, or "rippled scour depressions," within the Martha's Vineyard Coastal Observatory, Massachusetts. Cont. Shelf Res. 25 (4), 461–484.

Gooday, A.J., 1993. Deep-sea benthic foraminiferal species which exploit phytodetritus: characteristic features and controls on distribution. Mar. Micropaleontol. 22 (3), 187–205.

Gregory, D.D., Large, R.R., Halpin, J.A., Baturina, E.L., Lyons, T.W., Wu, S., Danyushevsky, L., Sack, P.J., Chappaz, A., Maslennikov, V.V., Bull, S.W., 2015. Trace element content of sedimentary pyrite in black shales. Econ. Geol. 110 (6), 1389–1410. https://doi.org/10.2113/econgeo.110.6.1389.

Hadden, C.S., Cherkinsky, A., 2015. 14C variations in pre-bomb nearshore habitats of the Florida Panhandle, USA. Radiocarbon 57 (3), 469–479.

Hayward, B.W., Hollis, C.J., 1994. Brackish foraminifera in New Zealand; a taxonomic and ecologic review. Micropaleontology 40 (3), 185–222.

Houser, T., 2008. Levelling the Carbon Playing Field: International Competition and US Climate Policy Design. Peterson Institute.

Kemp, A.C., Horton, B.P., Donnelly, J.P., Mann, M.E., Vermeer, M., Rahmstorf, S., 2011. Climate related sea-level variations over the past two millennia. Proc. Natl. Acad. Sci. 108 (27), 11017–11022.

Knutson, T.R., Sirutis, J.J., Garner, S.T., Held, I.M., Tuleya, R.E., 2007. Simulation of the recent multidecadal increase of Atlantic hurricane activity using an 18-km-grid regional model. Bull. Am. Meteorol. Soc. 88 (10), 1549–1565.
Knutson, T.R., Sirutis, J.J., Zhao, M., Tuleya, R.E., Bender, M., Vecchi, G.A., Villarini, G., Chavas, D., 2015. Global projections of intense tropical cyclone activity for the late twenty-first century from dynamical downscaling of CMIP5/RCP4. 5 scenarios. J. Clim. 28 (18), 7203–7224.
Kopp, R.E., Kemp, A.C., Bittermann, K., Horton, B.P., Donnelly, J.P., Gehrels, W.R., Hay, C.C., Mitrovica, J.X., Morrow, E.D., Rahmstorf, S., 2016. Temperature-driven global sea-level variability in the Common Era. Proc. Natl. Acad. Sci. 113 (11), E1434–E1441.
Kossin, J.P., Olander, T.L., Knapp, K.R., 2013. Trend analysis with a new global record of tropical cyclone intensity. J. Clim. 26 (24), 9960–9976.
Landsea, C.W., Harper, B.A., Hoarau, K., Knaff, J.A., 2006. Can we detect trends in extreme tropical cyclones? Science 313 (5786), 452–454.
Lane, P., Donnelly, J.P., Woodruff, J.D., Hawkes, A.D., 2011. A decadally-resolved paleohurricane record archived in the late Holocene sediments of a Florida sinkhole. Mar. Geol. 287 (1–4), 14–30.
Liu, K.B., Fearn, M.L., 2000. Reconstruction of prehistoric landfall frequencies of catastrophic hurricanes in northwestern Florida from lake sediment records. Quat. Res. 54 (2), 238–245.
Mamo, B.L., Brock, G.A., Gretton, E.J., 2013. Deep sea benthic foraminifera as proxies for palaeoclimatic fluctuations in the New Caledonia Basin, over the last 140,000 years. Mar. Micropaleontol. 104, 1–13.
Mann, R., Harding, J.M., Southworth, M.J., 2009. Reconstructing pre-colonial oyster demographics in the Chesapeake Bay, USA. Estuar. Coast. Shelf Sci. 85 (2), 217–222.
Milliken, K.T., Anderson, J.B., Rodriguez, A.B., 2008. A new composite Holocene Sea-level curve for the northern Gulf of Mexico. Geol. Soc. Am. Spec. Pap. 443 (1), 1–11.
Moore, L.J., List, J.H., Williams, S.J., Stolper, D., 2010. Complexities in barrier island response to sea-level rise: insights from numerical model experiments, North Carolina Outer Banks. J. Geophys. Res. 115, F03004.
Morton, R.A., 2002. Factors controlling storm impacts on coastal barriers and beaches: a preliminary basis for near real-time forecasting. J. Coast. Res. 486–501.
Morton, R.A., Barras, J.A., 2011. Hurricane impacts on coastal wetlands: a half-century record of storm-generated features from southern Louisiana. J. Coast. Res. 27 (6A), 27–43.
Morton, R.A., White, W.A., 1997. Characteristics of and corrections for core shortening in unconsolidated sediments. J. Coast. Res. 761–769.
Morton, R.A., Paine, J.G., Blum, M.D., 2000. Responses of stable bay-margin and barrier-island systems to Holocene Sea-level highstands, western Gulf of Mexico. J. Sediment. Res. 70 (3), 478–490.
Murray, J.W., 2006. Ecology and Applications of Benthic Foraminifera. Cambridge University Press.
National Hurricane Center, Hurricane Research Division; Atlantic Oceanographic and Meteorological Laboratory, 2012. Chronological List of All Continental United States Hurricanes: 1851–2011. United States National Oceanic and Atmospheric Administration's Office of Oceanic & Atmospheric Research.
Oehlert, A.M., Swart, P.K., 2014. Interpreting carbonate and organic carbon isotope covariance in the sedimentary record. Nat. Commun. 5 (1), 1–7.
Osterman, L.E., 2003. Benthic foraminifers from the continental shelf and slope of the Gulf of Mexico: an indicator of shelf hypoxia. Estuar. Coast. Shelf Sci. 58 (1), 17–35.
Otvos, E.G., 1982. Santa Rosa island, Florida panhandle, origins of a composite barrier island. Southeast. Geol. 23 (1), 15–23.
Otvos, E.G., 1985. Barrier platforms: northern Gulf of Mexico. Mar. Geol. 63 (1–4), 285–305.
Otvos, E.G., 2011. Hurricane signatures and landforms—toward improved interpretations and global storm climate chronology. Sediment. Geol. 239 (1–2), 10–22.
Otvos Jr., E.G., 1970. Development and migration of barrier islands, northern Gulf of Mexico. Geol. Soc. Am. Bull. 81 (1), 241–246.
Patterson, R.T., Fishbein, E., 1989. Re-examination of the statistical methods used to determine the number of point counts needed for micropaleontological quantitative research. J. Paleontol. 245–248.
Phleger, F.B., 1960. Ecology and Distribution of Recent Foraminifera, 1st ed. Johns Hopkins Press, p. 297.
Pielke Jr., R.A., Gratz, J., Landsea, C.W., Collins, D., Saunders, M.A., Musulin, R., 2008. Normalized hurricane damage in the United States: 1900–2005. Nat. Hazards Rev. 9 (1), 29–42.
Poag, C.W., 1981. Ecologic atlas of benthic foraminifera of the Gulf of Mexico. Marine Science International, Woods Hole, p. 174.
Poag, C.W., 2015. Benthic Foraminifera of the Gulf of Mexico: Distribution, Ecology, Paleoecology. Texas A&M University Press.
Rasmussen, P., Pantopoulos, G., Jensen, J.B., Olsen, J., Røy, H., Bennike, O., 2020. Holocene sedimentary and environmental development of Aarhus Bay, Denmark–a multi-proxy study. Boreas 49 (1), 108–128.
Reimer, P.J., Bard, E., Bayliss, A., Beck, J.W., Blackwell, P.G., Ramsey, C.B., Buck, C.E., Cheng, H., Edwards, R.L., Friedrich, M., Grootes, P.M., 2013. IntCal13 and Marine13 radiocarbon age calibration curves 0–50,000 years cal BP. Radiocarbon 55 (4), 1869–1887.
Reimnitz, E., Maurer, D.K., 1979. Effects of Storm Surges on the Beaufort Sea coast, northern Alaska. Arctic, pp. 329–344.
Roberts, M.L., von Reden, K.F., Burton, J.R., McIntyre, C.P., Beaupré, S.R., 2013. A gas-accepting ion source for Accelerator Mass Spectrometry: Progress and applications. Nucl. Instrum. Methods Phys. Res., Sect. B 294, 296–299.
Rodriguez, A.B., Meyer, C.T., 2006. Sea-level variation during the Holocene deduced from the morphologic and stratigraphic evolution of Morgan Peninsula, Alabama, USA. J. Sediment. Res. 76 (2), 257–269.
Rodriguez, A., Griffiths-Jones, S., Ashurst, J.L., Bradley, A., 2004. Identification of mammalian microRNA host genes and transcription units. Genome Res. 14 (10a), 1902–1910.
Rodysill, J.R., Donnelly, J.P., Sullivan, R., Lane, P.D., Toomey, M., Woodruff, J.D., Hawkes, A.D., MacDonald, D., d'Entremont, N., McKeon, K., Wallace, E., 2020. Historically unprecedented Northern Gulf of Mexico hurricane activity from 650 to 1250 CE. Sci. Rep. 10 (1), 1–17.
Ruth, B., Handley, L.R., 2006. Choctawhatchee Bay. In Seagrass status and trends in the northern Gulf of Mexico 1940–2002, pp. 143–153.
Sallenger Jr., A.H., 2000. Storm impact scale for barrier islands. J. Coast. Res. 890–895.
Santisteban, J.I., Mediavilla, R., Lopez-Pamo, E., Dabrio, C.J., Zapata, M.B.R., García, M. J.G., Castano, S., Martínez-Alfaro, P.E., 2004. Loss on ignition: a qualitative or quantitative method for organic matter and carbonate mineral content in sediments? J. Paleolimnol. 32 (3), 287–299.
Simms, A.R., Anderson, J.B., Milliken, K.T., Taha, Z.P., Wellner, J.S., 2007. Geomorphology and age of the oxygen isotope stage 2 (last lowstand) sequence boundary on the northwestern Gulf of Mexico continental shelf. Geol. Soc. Lond., Spec. Publ. 277 (1), 29–46.
Sobel, A.H., Camargo, S.J., Hall, T.M., Lee, C.Y., Tippett, M.K., Wing, A.A., 2016. Human influence on tropical cyclone intensity. Science 353 (6296), 242–246.
Stewart, L.B., Lagoe, M.B., Behrens, W., 1994. Late Holocene foraminiferal biofacies from Baffin Bay, Texas: preliminary analysis of a 4000-year record of paleosalinity. Gulf Coast Assoc. Geol. Soc. Trans. 44, 709–716.
Stuiver, M., Reimer, P.J., Reimer, R.W., 2020. CALIB 8.2 [WWW program] at. http://calib.org. accessed 2020-8-31.
Tanner, E.V.J., Kapos, V., Franco, W., 1992. Nitorgen and phosphorus fertilization effects on Venezuelan montane forest trunk growth and litterfall. Ecology 73 (1), 78–86.
Törnqvist, T.E., González, J.L., Newsom, L.A., Van der Borg, K., De Jong, A.F., Kurnik, C. W., 2004. Deciphering Holocene Sea-level history on the US Gulf Coast: a high-resolution record from the Mississippi Delta. GSA Bull. 116 (7–8), 1026–1039.
Törnqvist, T.E., Bick, S.J., van der Borg, K., de Jong, A.F., 2006. How stable is the mississippi delta? Geology 34 (8), 697–700.
Törnqvist, T.E., Jankowski, K.L., Li, Y.X., González, J.L., 2020. Tipping points of Mississippi Delta marshes due to accelerated sea-level rise. Sci. Adv. 6 (21) eaaz5512.
Tsandev, I., Rabouille, C., Slomp, C.P., Cappellen, P.V., 2010. Shelf erosion and submarine river canyons: implications for deep-sea oxygenation and ocean productivity during glaciation. Biogeosci. Discuss. 7 (1), 879.
Van Hengstum, P.J., Reinhardt, E.G., Beddows, P.A., Huang, R.J., Gabriel, J.J., 2008. Thecamoebians (testate amoebae) and foraminifera from three anchialine cenotes in Mexico: Low salinity (1.5–4.5 psu) faunal transitions. The J. Foraminif. Res. 38 (4), 305–317.
Wang, P., Kirby, J.H., Haber, J.D., Horwitz, M.H., Knorr, P.O., Krock, J.R., 2006. Morphological and sedimentological impacts of Hurricane Ivan and immediate poststorm beach recovery along the northwestern Florida barrier-island coasts. J. Coast. Res. 22 (6), 1382–1402.
Ward Jr., J.H., 1963. Hierarchical grouping to optimize an objective function. J. Am. Stat. Assoc. 58 (301), 236–244.
Webster, P.J., Holland, G.J., Curry, J.A., Chang, H.R., 2005. Changes in tropical cyclone number, duration, and intensity in a warming environment. Science 309 (5742), 1844–1846.